Eye features and retinal photoreceptors of the nocturnal aardvark (*Orycteropus afer*, Tubulidentata)

Leo Peichl[1,2*] (ORCID ID: 0000-0002-8141-0911), Sonja Meimann[2], Irina Solovei[3] (ORCID ID: 0000-0002-6813-7279), Irene L. Gügel[4] (ORCID ID: 0000-0002-5475-9210), Christina Geiger[5], Nicole Schauerte[5], Karolina Goździewska-Harłajczuk[6] (ORCID ID: 0000-0003-4412-1966), Joanna E. Klećkowska-Nawrot[6] (ORCID ID: 0000-0003-1154-8736), Gudrun Wibbelt[7] (ORCID ID: 0000-0002-3456-1303), Silke Haverkamp[4] (ORCID ID: 0000-0003-3084-6544)

[1]Institute for Clinical Neuroanatomy, Dr. Senckenbergische Anatomie, Goethe University, Frankfurt am Main, Germany.
[2]Institute of Cellular and Molecular Anatomy, Dr. Senckenbergische Anatomie, Goethe University, Frankfurt am Main, Germany.
[3]Biozentrum, Ludwig Maximilians University Munich, Planegg-Martinsried, Germany.
[4]Department of Computational Neuroethology, Max Planck Institute for Neurobiology of Behavior - Caesar, Bonn, Germany.
[5]Zoo Frankfurt, Frankfurt am Main, Germany.
[6]Department of Biostructure and Animal Physiology, Faculty of Veterinary Medicine, Wrocław University of Environmental and Life Sciences, Wrocław, Poland.
[7]Department of Wildlife Diseases, Leibniz Institute for Zoo and Wildlife Research, Berlin, Germany

Short title: Aardvark eye and retinal photoreceptors

Keywords: Mammal, vision, tapetum lucidum, cone photoreceptor, rod photoreceptor, opsin coexpression, thyroid hormones

*Corresponding author:
peichl@em.uni-frankfurt.de

Abstract

The nocturnal aardvark *Orycteropus afer* is the only extant species in the mammalian order Tubulidentata. Previous studies have claimed that it has an all-rod retina. In the retina of one aardvark, we found rod densities ranging from 124,000/mm² in peripheral retina to 214,000/mm² in central retina; the retina of another aardvark had 182,000 – 245,000 rods/mm². This is moderate in comparison to other nocturnal mammals. With opsin immunolabelling we found that the aardvark also has a small population of cone photoreceptors. Cone densities ranged from 300 to 1,300/mm² in one animal, and from 1,100 to 1,600/mm² in the other animal, with large local variations and no large central-peripheral density gradient. Overall, cones comprised 0.25-0.9% of the photoreceptors. Both typical mammalian cone opsins, longwave-sensitive (L) and shortwave-sensitive (S), were present. However, there was colocalization of the two opsins in many cones across the retina (35 – 96% dual pigment cones). Pure L cones and S cones formed smaller populations. This probably results in poor colour discrimination. Thyroid hormones, important regulators of cone opsin expression, showed normal blood serum levels. The relatively low rod density and hence a relatively thin retina may be related to the fact that the aardvark retina is avascular and its oxygen and nutrient supply have to come from the choriocapillaris by diffusion. In contrast to some previous studies, we found that the aardvark eye has a reflective tapetum lucidum with features of a choroidal tapetum fibrosum, in front of which the retinal pigment epithelium is unpigmented. The discussion considers these findings from a comparative perspective.

Introduction

The aardvark (*Orycteropus afer*) is the only extant species of the order Tubulidentata in the supraordinal mammalian clade Afrotheria. It is a medium-sized, pig-like mammal native to sub-Saharan Africa (Fig 1). The aardvark is a nocturnal, burrowing species that mostly feeds on ants and termites (for an overview, see, e.g., [1,2]). The strong legs with sharp claws are used to dig out termite and ant nests, as well as abode burrows; the genus name *Orycteropus* means 'burrowing foot.' The aardvark is considered a 'living fossil,' because *Orycteropus* fossils from about 20 million years ago show nearly identical morphological features to those of living aardvarks [2]. It is assumed that aardvarks have an acute sense of smell and hearing, but poor eyesight. However, in contrast to the abundant literature available on the eyes and retinae of many other mammals, the only substantial study of the aardvark retina known to us is that of Victor Franz, published in 1909 [3]. Franz obtained the two eyes of one animal hunted at a zoological expedition and examined them in detail macroscopically and microscopically. The study contains much valuable information, but also some apparent errors, most likely due to the histological methods available at the time. Franz [3] reports a complete absence of cone photoreceptors in the retina, which appears doubtful in the light of more recent research demonstrating cones in nearly all mammals studied to date (reviews: [4,5]). Among the few exceptions without functional cones are some deep-diving whales [6], the subterranean golden moles [7], and Xenarthra [8]. Franz [3] also states that the aardvark has no reflective tapetum lucidum. In contrast, a recent study of the orbital structures and eye tunics of young and adult aardvarks reports the presence of a tapetum lucidum [9]. Nocturnal photographs of aardvarks show a strong eyeshine or 'glow' (Fig 1). However, this could also be a reflection off the fundus like the 'red eye effect' seen, e.g., in human eyes in flash photographs. When we obtained the relatively well-preserved eyes of two aardvark individuals, we studied them with currently available histological approaches to resolve the

above discrepancies and to add new observations on aardvark retinal anatomy. The present paper reports on general eye features and the photoreceptors. A separate paper shall describe aardvark retinal bipolar cells, horizontal cells, amacrine cells and ganglion cells.

Fig 1. Aardvarks at day and night, note the laterally positioned eyes. (**A**) Aardvark 1, the *post mortem* donor of the studied eye, at daytime. (**B, C**) Another aardvark, flashlight photographs taken at night. When the head is viewed horizontally, there is a bright whitish eyeshine indicating a tapetum lucidum; when viewed from above, the weaker eyeshine appears orange to red. For details see text. Image sources: (A) Frankfurt Zoo; (B, C) Christina Geiger.

Methods

Tissue

This study has used tissue from aardvarks (*Orycteropus afer*) that was obtained from zoo animals that had died of natural causes. The aardvark IUCN status is 'least concern' and no ethical approval was required for use of the tissue. The right eye of a nearly 25 years old male aardvark was obtained when the animal died of old age in the Zoo of Frankfurt am Main, Germany. The animal is termed "aardvark 1" here (Fig 1A). It had an age-related cataract and a mild chronic *Uveitis anterior*, but the retina appeared macroscopically normal. One day post mortem, the eye was enucleated during autopsy, punctured behind the cornea for better fixative penetration, and immersion-fixed in 4% formalin for 24 h at 4°C. When punctured, the eye lost some liquefied vitreous and aqueous humor, leading to a collapse of the cornea and a slight deformation of the eyeball during fixation. After fixation the external eye dimensions were recorded, the eye was cut open behind the cornea, and the posterior eyecup with attached retina was washed in 0.01M phosphate buffered saline (PBS, pH 7.4). The

retina was carefully dissected from the eyecup after having marked its orientation. It was cryoprotected by successive immersion in 10%, 20% and 30% (w/v) sucrose in phosphate buffer (PB, pH 7.4) containing 0.05% sodium azide, and stored frozen at -20°C until further processing. The eyecup was stored in PBS with 0.05% sodium azide at 4°C.

The eyes of a nearly 6 years old female aardvark were obtained when the animal died of perinatal complications in the Zoological Garden of Wrocław (Poland). The animal is termed "aardvark 2" here, it was genetically unrelated to aardvark 1. The eyes were enucleated immediately post mortem and immersion-fixed in 4% buffered formaldehyde solution, they have been used in a previous study of aardvark eye and orbital features [9]. The right eye was kept in the fixative for 1 week and then embedded in paraffin for sectioning. The left eye was permanently stored in the fixative, and only small pieces of the retina were available for the present study. Probably due to the long fixation time of this eye (ca. 7 years), some of the antibodies used here did not work (see below and Results).

For frozen vertical sections of the retina (i.e., perpendicular to the retinal layers), pieces of retina were transferred from 30% sucrose to tissue freezing medium (Leica Biosystems, Wetzlar, Germany), frozen, sectioned at 16 µm thickness with a cryostat (Leica CM 3050 S, Wetzlar, Germany), and collected on Superfrost Plus slides (Menzel Gläser, Braunschweig, Germany).

For electron microscopy, small pieces of the sclera and presumed tapetum lucidum were stained as previously described [10]. Briefly, the samples were stained in a solution containing 1% osmium tetroxide, 1.5% potassium ferrocyanide, and 0.15 M cacodylate buffer. The osmium stain was amplified with 1% thiocarbohydrazide and 2% osmium tetroxide. The tissue was then stained with 2% aqueous uranyl acetate and lead aspartate. The

134 tissue was dehydrated through an 70%–100% ethanol series, transferred to propylene oxide,
135 infiltrated with 50%/50% propylene oxide/epon medium hard formulation (EMbed 812,
136 Electron Microscopy Sciences; [11]), and then 100% epon medium hard. The epon medium
137 hard infiltrated tissue was transferred into multi-well embedding molds (Electron Microscopy
138 Sciences) and hardened at 60°C. For scanning electron microscopy (SEM), a few serial
139 sections of 50 nm were taken with a Diatome ultra diamond knife and collected on glow
140 discharged silicon wafers and dried on a heating plate at 50 °C until the water was fully
141 evaporated. The wafers were mounted with silver paint (Plano) on a sample holder and
142 images were taken with a Supra55 (Leica) SEM. For transmission electron microscopy
143 (TEM), 50-nm-thick sections were cut with an Ultra diamond knife and transferred on carbon-
144 coated copper grids with a hole size of 35/10 nm (S35/10, Quantifoil, Electron Microscopy
145 Sciences). Images were recorded with an analytical electron microscope (JEM-2200FS, Jeol)
146 at an energy of 200 keV with a CMOS camera (TEM-CAM F416, TVIPS).
147
148 For comparison of the choroid, vertical cryo-sections of the formalin-fixed eye of a captive
149 adult African elephant (*Loxodonta africana*) from a German zoo was used. In agreement with
150 CITES regulations the eye was collected during necropsy for pathological investigations
151 performed by the Institute for Zoo and Wildlife Research, Berlin (IZW) after the animal had
152 to be euthanized because of severe disease unresponsive to treatment.
153
154 *Immunohistochemistry*
155 Immunohistochemistry was performed on vertical sections of the retina, as well as on
156 unsectioned retinal pieces from various regions to assess cell populations in flat view.
157 Immunolabelling followed standard protocols. Briefly, sections on the slide and free-floating
158 pieces were preincubated for 1 h in PB with 0.5% Triton X-100 and 10% normal donkey
159 serum (NDS). Incubation in the primary antibody/antiserum solution, made up in PB with 3%

160 NDS and 0.5% Triton X-100, was overnight at room temperature for sections, and 3 days at
161 room temperature or 4 days at 4°C for unsectioned pieces. Multiple immunofluorescence
162 labelling for simultaneous visualization of several antigens was performed by incubation in a
163 mixture of the antisera. Table 1 lists all primary antibodies used. The cone opsin antisera
164 JH492, JH455 and sc-14363 have been used in several previous studies to reliably label the
165 respective opsins in a range of mammals [12-16].
166

167 **Table 1. Primary antibodies and cell markers used**

Antigen / marker	Immunogen / target structure	Antibody host species, catalog #, RRID	Dilution	Source
Rod opsin	N-terminal region of bovine rhodopsin[1]	Mouse monoclonal, Name: rho4D2, RRID: AB_2315273	1:1000	Gift of R. S. Molday, University of British Columbia Life Sciences Centre, Vancouver, Canada
L cone opsin	C-terminal 38 amino acids of human red cone opsin[2]	Rabbit polyclonal, Name: JH 492, RRID: AB_2315259	1:2,000	Gift of J. Nathans, Johns Hopkins University School of Medicine, Baltimore, Maryland, USA
S cone opsin	C-terminal 42 aa of human blue cone opsin[2]	Rabbit polyclonal, Name: JH 455, RRID: AB_2313807	1:5,000	Gift of J. Nathans, Johns Hopkins University School of Medicine, Baltimore, Maryland, USA
S cone opsin	20 aa peptide mapping near N-terminus of human blue cone opsin[3]	Goat polyclonal, Cat# sc-14363, RRID: AB_2158332	1:500	Santa Cruz Biotechnology
CtBP2 (C-Terminal Binding Protein-2)	Mouse CtBP2, aa. 361-445	Mouse monoclonal, Cat# 612044, RRID: AB_399431	1:5000	BD Biosciences
CtBP2	Rat CtBP2, aa 431-445	Rabbit polyclonal, Cat# 193 003, RRID: AB_2086768	1:5000	Synaptic Systems
GS (Glutamine synthetase)	Müller glia	Mouse monoclonal, Cat# 610517, RRID: AB_397879	1:500	BD Bioscience
GFAP	Glial fibrillary acidic protein	Mouse monoclonal, Cat# G3893, RRID: AB_477010	1:500	Sigma-Aldrich
H3K4me3	Euchromatin	Rabbit polyclonal, Cat# ab8580,	1:500	abcam

		RRID: AB_306649		
H4K20me3	Heterochromatin	Mouse monoclonal, CMA423	1:500	Generated in Hiroshi Kimura' lab, Tokyo University
Lamins A/C	Inner nuclear membrane protein	Mouse serum	Undiluted	Gift of Harald Herrmann, German Cancer Research Center
LBR	Inner nuclear membrane protein	Guinea pig serum	1:50	Generated in Harald Herrmann's lab, German Cancer Research Center
PNA-647 (Peanut agglutinin)	General cone marker	Cat# L-32460	1:100	Molecular Probes
NeuN	Synthetic peptide NeuN	Rabbit monoclonal (EPR12763), Cat# ab177487, RRID: AB_2532109	1:100	abcam
NeuroTrace (Ex 530 / Em 615)	Fluorescent Nissl stain	Cat# N-21482	1:100	Molecular Probes
Isolectin B4, biotinylated	Blood vessel marker	Cat# B-1205	1:50	Vector Laboratories

[1]Ref. [86], [2]Ref. [87], [3]Ref. [12].

Binding sites of the primary antibodies were visualized by indirect immunofluorescence, with a 1.0-1.5 h incubation of the tissue in the secondary antiserum, or in a mixture of appropriate secondary antisera in the case of several primary antibodies. We used secondary antisera conjugated to Alexa 488, Alexa 647, Cy3 and Cy5 in appropriate combinations. Omission of the primary antibodies from the incubation solution resulted in no staining. In addition to antisera, we used the fluorescent markers peanut agglutinin (PNA) and NeuroTrace for certain cell types (Table 1). After immunolabelling, sections were incubated in a solution of 4,6-diamidino-2-phenylindole (DAPI) as a fluorescent nuclear stain to reveal the general retinal layering. Choroidal blood vessels were labeled by biotinylated isolectin B4 (Table 1; incubation was 1 h for sections, 2 h for unsectioned pieces) and visualized by a subsequent 1.0-1.5 h incubation in streptavidin coupled to Alexa 549 or 488. Tissue was coverslipped with an aqueous mounting medium (AquaPoly/Mount, Polysciences Inc., Warrington, PA, USA; or Dako Fluorescence Mounting Medium S3032, Dako North America Inc., Carpinteria, CA, USA).

184

185 In retinal pieces from the long-fixed eye of aardvark 2, the S cone opsin antiserum sc14363
186 did not work, hence assessment of the cone opsin pattern was done by sequential double-
187 labeling with the two rabbit antisera JH492 against the L cone opsin and JH455 against the S
188 cone opsin as follows. One retinal piece was first incubated in a JH492 solution and then in a
189 donkey-anti-rabbit antiserum conjugated to Alexa 488. Then the piece was incubated in a
190 JH455 solution and finally in a donkey-anti-rabbit antiserum conjugated to Cy3. This
191 secondary antiserum bound to both primary antisera, hence all cones were labeled by Cy3.
192 The cones also labeled by Alexa 488 were those that contained L cone opsin, and cones only
193 labeled by Cy3 were pure S cones. In a neighboring piece of retina, the order of labeling was
194 reversed: First incubation in the JH455 solution and visualization with the donkey-anti-rabbit
195 antiserum conjugated to Alexa 488, then incubation in the JH492 solution and visualization
196 with the donkey-anti-rabbit antiserum conjugated to Cy3. Again, all cones were labeled by
197 Cy3, but here the cones also labeled by Alexa 488 were those that contained S cone opsin, and
198 those only labeled by Cy3 were pure L cones. Combining the data from the two pieces
199 provided the total cone density, the percentages of pure L and S cones, and the proportion of
200 cones containing L and S opsin, from which the percentage of dual pigment cones could be
201 calculated for that retinal region.

202

203 For assessment of the retinal vascularization, a retinal piece of 5.5 x 4.0 mm size containing
204 the optic nerve head was stained with a 3,3'-diaminobenzidine (DAB) reaction to selectively
205 visualize the endogenous peroxidase in the vasculature. The retinal piece was washed in
206 0.05% Tris buffer (TRIS, pH 7.6), then incubated for 20 min in a solution of 0.05% DAB in
207 TRIS, after which hydrogen peroxide was added to the incubation solution at a final
208 concentration of 0.01%, and the incubation was continued for 10 min until the peroxidase
209 reaction had fully developed. The reaction was stopped by several washes in TRIS and then

210 PB. The retinal piece was flat-mounted on a slide and coverslipped with AquaPoly/Mount.
211 For assessment of the retinal pigment epithelium (RPE) after removal of the retina, pieces of
212 the thin RPE layer from the central and peripheral fundus were gently removed from the
213 underlying tissue, flat-mounted on a slide and coverslipped with AquaPoly/Mount.
214
215 *Imaging and analysis*
216 The RPE and the DAB-labelled vasculature of the optic nerve head were analyzed with a
217 Zeiss Axioplan 2 microscope by differential interference contrast. Micrographs were taken
218 with a CCD camera and the Axiovision LE software (Carl Zeiss Vision, Germany). The
219 immunofluorescence-labelled sections and retinal pieces were analyzed with a laser scanning
220 microscope (LSM) Olympus FluoView 1000 using the FV 1.7 software (Olympus), or with a
221 Leica TCS SP5 or a Leica TCS SP8 confocal microscope. LSM images and z-stack
222 projections were examined with ImageJ (https://imagej.net); cells were counted using the cell
223 counter plugin. Images for illustration were adjusted for brightness and contrast using Adobe
224 Photoshop. Irrespective of the fluorescent dye used to visualize a label, labels are shown in
225 the RGB channels that are most suitable to illustrate label combinations. For the benefit of
226 red/green-blind readers, combinations of magenta and green are preferred over red and green.
227
228 *Thyroid hormone*
229 Thyroid hormone (TH), via its receptor TRβ2, is an important regulator of cone spectral
230 identity by repressing S opsin and activating L opsin in developing and adult retina (see
231 Discussion). Because of the L and S opsin co-expression in a large proportion of the aardvark
232 cones, we were interested to know whether the serum TH levels in aardvark differ from those
233 in other mammals. Frankfurt Zoo, during medical check-ups, had obtained five blood counts
234 of aardvark 1 over the last three years of his life, and one blood count of his 21 years old son
235 (here termed “aardvark 3”), all including serum TH levels. The blood analysis was done by

236 the commercial veterinary clinical diagnostics laboratory LABOKLIN (Bad Kissingen,
237 Germany).
238
239 **Results**
240 Most findings reported here came from aardvark 1. The retina of aardvark 2 was used for
241 comparison of the photoreceptor findings.
242
243 *General eye features*
244 The eye of aardvark 1 had an equatorial diameter of ca. 23.0 mm and an axial length of ca.
245 21.2 mm. The axial length probably is an underestimate because the cornea had collapsed and
246 its original curvature was estimated (Fig 2A). The cornea was elliptical with a naso-temporal
247 diameter of 18.8 mm and a dorso-ventral diameter of 15.5 mm (mean 17.1 mm); the ratio of
248 mean corneal diameter to eye equatorial diameter was 0.75, and the ratio of mean corneal
249 diameter to eye axial length was 0.81. The lens diameter was 13.3 mm and the lens thickness
250 9.5 mm (Fig 2B). The curvature was stronger at the posterior than at the anterior side of the
251 lens (not illustrated). The ratio of lens diameter to eye equatorial diameter was 0.58, the ratio
252 of lens thickness to eye axial length was 0.45. The poor pigmentation of the choroid and
253 sclera in the present eye confirms the observations by Franz [3].
254
255 **Fig 2. General eye features** (aardvark 1). (**A**) Intact eye, frontal view with attached rectus
256 muscles. The cornea had collapsed when the eye was punctured for better fixative penetration
257 to the retina. (**B**) Anterior part of the opened eye from the vitreous side, showing the lens and
258 ciliary body. (**C**) Opened eyecup showing the fundus with the retina in situ. There is a light
259 horizontal band where the retinal pigment epithelium (RPE) is weakly pigmented or
260 unpigmented. The transition to the pigmented peripheral RPE is gradual at the dorsal side and
261 with a rather sharp boundary at the ventral side. (**D**) Eyecup after removal of the retina. Some

262 RPE also came off during the preparation, showing an unpigmented, whitish-yellow choroid.
263 The optic disc (OD) is located ventral to the light horizontal band of (C). (**E**) Optic disc in the
264 isolated retina, DAB-reacted for blood vessels. There are only a few capillaries present in the
265 optic disc (arrow heads), and no blood vessels exit it to supply the surrounding retina. Around
266 the optic disc there is an accumulation of pigment. (**F, G**) Light microscopic images of flat-
267 mounted RPE pieces from peripheral (F) and central fundus (G). In the periphery, all RPE
268 cells contain densely packed melanin granules (F); centrally, only very few RPE cells are rich
269 in melanin granules, the vast majority of RPE cells contains little or no melanin (G). Eye
270 dimensions in (A, C, D) can be determined from the millimeter graph paper in (C). The scale
271 bar in (F) applies to (F, G). d, dorsal; n, nasal; t, temporal, v, ventral.
272
273 The fundus in the opened eyecup showed a bright yellowish band extending from the
274 temporal to the nasal periphery. This bright band had the appearance of a tapetum lucidum, its
275 dorso-ventral width was larger in the temporal than the nasal fundus. Its relatively sharp
276 ventral boundary ran along the horizontal midline of the fundus, its dorsal boundary showed a
277 more gradual transition to the pigmented part of the fundus (Fig 2C, D). The ventral half and
278 the dorsal periphery of the fundus were covered by brown-black retinal pigment epithelium
279 (RPE). The optic nerve head (optic disc, OD) was located centrally on the temporal-nasal eye
280 axis and ventral to the geometric center of the eyecup, about one OD diameter below the
281 ventral boundary of the bright fundus band (Fig. 2D). When the retina was removed, the
282 remaining thin RPE layer consisted of RPE cells (melanocytes) that contained a high density
283 of melanin granules in the dark-appearing parts of the fundus (Figs 2D, F, 3A). In the central
284 bright-appearing band, the large majority of RPE cells contained very few or no melanin
285 granules, and only some single cells or small cell clusters contained ample melanin (Figs 2G,
286 3A). The absence of pigmentation in a horizontal band of the central fundus and the
287 associated tapetum-like reflection explain the eyeshine differences seen at different angles

288 (Fig 1B, C). When the eye is seen horizontally, the strong reflectivity of this band produces a
289 bright whitish to yellowish eyeshine. When the eye is seen from above, the lower reflectivity
290 of the more pigmented ventral fundus produces a fainter orange to red eyeshine that resembles
291 the 'red eye effect' seen in flash photographs of human eyes with their pigmented fundus.
292
293 **Fig 3. Choroid and tapetum lucidum** (aardvark 1). (**A**) Higher power view of the central
294 and ventral midperipheral fundus of the aardvark eye (c.f. Fig. 1). Below the partly removed
295 RPE layer, the whitish unpigmented choroid with its red blood vessels is visible. (**B**) SEM
296 micrograph of subcellular structures from the RPE-facing side of a transverse choroid section,
297 showing collagen fibrils arranged in parallel bundles with different orientations that indicate a
298 tapetum lucidum. In the upper image part, the fibrils are longitudinally sectioned; in the
299 bottom image part, they are cross-sectioned with round to oval profiles. (**C**) At higher
300 magnification, the fibrils show the typical cross-striation of native collagen (TEM image). (**D**)
301 In cross-section, the fibrils show a shell and core of higher electron density (SEM image). (**E**)
302 Differential interference contrast (DIC) image of a vertical cryo-section of the aardvark
303 choroid (Ch) and tapetum (Tap). The poorly pigmented choroid shows cross-sections of blood
304 vessels of various calibers, the tapetum shows a horizontal striation indicating tapetal laminae.
305 (**F**) DIC image of a vertical cryo-section of the choroid and tapetum of an African elephant
306 for comparison. The choroid is strongly pigmented, and the tapetum is thicker and more
307 conspicuously striated than in the aardvark. (**G**) Aardvark vertical cryo-section of the choroid
308 and tapetum with blood vessel labelling by isolectin (red). The choroid part contains vessels
309 of larger and smaller caliber, the tapetum layer is relatively thin, and the choriocapillaris at the
310 border to the RPE is densely filled with capillaries. (**H**) African elephant vertical cryo-section
311 of the choroid and tapetum with blood vessel labelling by isolectin (red) for comparison. The
312 image shows a vertical choroidal blood vessel supplying the CC capillaries. For the sections
313 of (E-H), the choroid has been removed from the sclera, so the sections do not show the full

314 thickness of the choroid. (**I**) Flat view of the aardvark choriocapillaris, labelled by isolectin
315 (red) and showing the dense capillary net. The scale bar in (E) applies to (E, F), the scale bar
316 in (G) applies to (G-I).
317
318 *Choroid and tapetum lucidum*
319 Once the retina was removed, the thin RPE layer readily detached from the choroid in shreds
320 (Figs 2D, 3A). The strongly vascularized choroid was unpigmented and appeared whitish with
321 a mother-of-pearl-like reflection throughout the fundus; in the fundus regions with pigmented
322 RPE, this choroidal reflection was concealed (Fig 3A). Electron microscopy of transverse
323 choroid sections showed that at the RPE-facing side of the choroid, there were fibrillar
324 structures arranged in parallel, with different orientations in neighbouring domains (Fig 3B).
325 In some domains the fibrils were densely packed, in others they were less dense or sparse.
326 Fibril diameters seen in cross-sections were 120-310 nm, being 150-250 nm in most cases.
327 Observed fibril lengths were up to about 7 µm. In TEM images, the fibrils showed the typical
328 cross-striation of native collagen, indicating a choroidal tapetum lucidum fibrosum (Fig 3C).
329 However, in SEM images, cross-sections of the fibrils showed a substructure with a more
330 electron-dense shell and core, which is more characteristic of the rodlets of a tapetum
331 cellulosum (Fig 3D). This is addressed in the Discussion. Overall, the presumed tapetum layer
332 is thinner and less conspicuously striated than, e.g., in the African elephant, like the aardvark
333 a member of the Afrotheria with an avascular retina (Fig 3E, F). The boundary of the choroid
334 and tapetum to the RPE is formed by the choriocapillaris, a dense capillary net that was
335 labelled by the endothelial cell marker isolectin B4 in vertical sections of both aardvark (Fig
336 3G) and African elephant (Fig 3H). The dense mesh of the aardvark choriocapillaris is
337 particularly obvious in flat view (Fig 3I).
338
339 *General Retina Features*

340 We confirm that the aardvark retina is avascular. In the fundus, there were no obvious blood
341 vessels emerging from the optic disc or extending across the retina. Staining of blood vessels
342 with DAB in a piece of central retina containing the optic disc revealed a few small capillaries
343 within the optic disc and confirmed that there were no blood vessels extending outside the
344 optic disc and into the retina (Fig 2E).
345
346 In the vertical sections, retinal thickness ranged from ca. 120 µm to ca. 180 µm. This is an
347 estimate, given the fact that the sections may not be exactly vertical and that the length of
348 photoreceptor outer segments may not be fully preserved. The layering of the aardvark retina
349 conformed to the typical mammalian pattern (Fig 4). The outer nuclear layer (ONL) with the
350 photoreceptor somata was the thickest layer, indicating a dominance of rod photoreceptors,
351 which is the situation seen in most mammals. The ONL had six to nine soma tiers in more
352 central retina and five to seven tiers in more peripheral retina. The inner nuclear layer (INL)
353 had three to four soma tiers in central retina and two to three soma tiers in peripheral retina.
354 The ganglion cell layer (GCL) was sparsely populated by somata. The narrower outer
355 plexiform layer (OPL) and broader inner plexiform layer (IPL) separated the soma layers.
356
357 **Fig 4. General retinal features** (aardvark 1). (**A**) Overview of a vertical retinal section
358 labelled with the fluorescent Nissl stain NeuroTrace, revealing the retinal layering. Cell
359 bodies in the outer nuclear layer (ONL) and inner nuclear layer (INL) are stacked in several
360 tiers. The photoreceptor outer and inner segments (OS+IS) are also labelled. The ganglion cell
361 layer (GCL) is sparsely populated by cells of various soma sizes. A large soma of a putative
362 alpha cell is marked by an arrowhead. (**B, C**) Double labelling with an antibody against the
363 neuronal marker NeuN and with NeuroTrace. NeuN only labels a few presumed amacrine cell
364 somata in the INL and some somata in the GCL (B). The NeuroTrace counterstain shows the
365 position of the NeuN somata in the layers (C). (**D, E**) Immunolabelling for glutamine

366 synthetase shows the Müller cells forming the retinal glia scaffold (D). Counterstaining with
367 DAPI (E) shows that the Müller cells have their somata in the INL and vertically extend their
368 processes from the inner limiting membrane (ILM) formed by their endfeet to the outer
369 limiting membrane (OLM). The images are maximum intensity projections of confocal image
370 stacks. OPL, outer plexiform layer; IPL, inner plexiform layer. Scale bars are 100 µm, scale
371 bar in (C) applies to (B-E).
372
373 Müller cells, the scaffolding radial macroglia of the retina, were specifically labelled by an
374 antibody against glutamine synthetase (Fig 4D, E). They were present at a high density and
375 had the mammalian-typical morphology. Their somata were located in the INL. Their inward
376 processes traversed the IPL and terminated in the Müller cell endfeet that ended at the inner
377 limiting membrane (ILM), separating the retina from the vitreous. In some of the cells these
378 processes bifurcated and formed two endfeet. Their outward processes encircled the
379 photoreceptor somata in the ONL and ended at the outer limiting membrane (OLM) that lies
380 between the ONL and the photoreceptor inner segments. An antibody against glial fibrillary
381 acidic protein (GFAP) did not label any structures (not illustrated). Hence, there are no
382 astrocytes in the aardvark retina, as mammalian astrocytes specifically express GFAP [17].
383 This is in line with the absence of retinal blood vessels (see Discussion). Furthermore, the
384 absence of GFAP label in the Müller cells indicates that the studied retina was healthy. The
385 Müller cells of healthy retinae have very low or no GFAP expression, but show reactive
386 gliosis with dramatically upregulated GFAP expression to practically all forms of retinal
387 stress, i.e. to various retinal diseases and injuries (reviews: [18,19].
388
389 *Rod photoreceptors*
390 In the retina of aardvark 1, rod photoreceptors were identified by labelling with an antibody to
391 rod opsin (Fig 5A, B), and by their characteristic nuclear morphology (Fig 5C, D). Their outer

392 segments showed the most intense rod opsin label and formed a densely packed layer at the
393 outer retinal surface (Fig 5A). The used antibody rho4D2 also, but less intensely, labelled the
394 other parts of the rod cells, particularly the soma cytoplasm in the ONL and the axonal ending
395 in the OPL (Fig 5B), which is common in mammals. The large majority of the photoreceptor
396 somata in the ONL showed rho4D2 label and hence are rod somata. This fits the very low
397 aardvark cone densities (see below).
398
399 **Fig 5. Rod photoreceptors** (aardvark 1). (**A, B**) Vertical retinal section, rod opsin label
400 (green). (**A**) The rod outer segments are strongly labelled, DAPI counterstaining (blue) shows
401 the retinal nuclear layers. (**B**) Overexposure of the same field shows less strong opsin label in
402 the rod somata in the outer nuclear layer (ONL) and the rod axonal spherules in the outer
403 plexiform layer (OPL). Clearly, the vast majority of ONL somata belong to rods. (**C-G**) DAPI
404 nuclear staining of various retinal neurons to reveal their heterochromatin arrangement. (**C**)
405 Overview of a DAPI stained section, nuclei in the ONL (top) are more intensely stained than
406 those in the INL (middle) and GCL (bottom), confirming the appearance seen in (A). (**D**) The
407 rod nuclei show a "semi-inverted" nuclear architecture with most of the heterochromatin
408 clustered in the nuclear centre, often in two aggregates, but with some extensions towards the
409 nuclear periphery. (**E**) In contrast, the cone nuclei (arrowhead) have several smaller
410 heterochromatin clusters localized towards the nuclear periphery (conventional nuclear
411 architecture). The same conventional heterochromatin arrangement is seen in cells of the INL
412 (**F**) and in retinal ganglion cells (**G**). (**H**) In the rods, euchromatin (immunolabelled by anti-
413 H3K4me3, green) is located mostly in the nuclear periphery and in the gaps between the
414 heterochromatin clusters (DAPI, red). (**I**) In the rod nuclei, heterochromatin (immunolabelled
415 by anti-H4K20me3, green) colocalizes with the DAPI staining (red), the merge of the labels
416 appears yellow. (**J-L**) Immunolabelling for lamin A/C (red) and LBR (green), counterstained
417 with DAPI (blue). The aardvark retina shows a presence of lamin A/C in the neuronal nuclei

418 in all layers (**J, K**). As a positive control for labeling with the anti-LBR antibody, the nucleus
419 of a microglial cell (arrowhead) expressing LBR but not lamin A/C is shown in (K). LBR
420 label is only present in microglial cells, not in any neurons. (**L**) A rod nucleus (left) and a
421 cone nucleus (right, arrowhead) with labelled lamin A/C. For layer abbreviations, see Fig 3.
422 Scale bar in (B) applies to (A, B).
423
424 In the vast majority of eukaryotic cells, the euchromatin is located in the centre of the nucleus
425 and the heterochromatin in the nuclear periphery. In contrast, the rod nuclei of nocturnal
426 mammals have a unique inverted chromatin architecture with heterochromatin aggregated in
427 the nuclear centre and euchromatin arranged at the nuclear periphery. This unusual chromatin
428 arrangement evolved as an adaptation to night vision because it reduces light scattering in the
429 thick retinae of nocturnal species, enhancing their ability to detect low intensity light [20-22].
430 In the nocturnal aardvark, the heterochromatin in the rods was clustered in two large central
431 granules, thus the nuclei seem to be inverted (Fig 5D, H, I). At the same time, the internal
432 heterochromatin exhibited several protrusions towards the nuclear envelope (Fig 5D), making
433 these nuclei semi-inverted. All other retinal cells, including the cones, had the conventional
434 nuclear architecture with heterochromatin attached to the nuclear periphery or nucleolus (Fig
435 5E-G). The nuclear envelope protein lamin A/C was present in all retinal nuclei including the
436 rod nuclei, whereas the lamin B receptor (LBR) of the nuclear envelope was only present in
437 retinal microglial cells, not in any retinal neurons (Fig 5J-L). The functional implications of
438 the nuclear inversion and the role of nuclear envelope proteins in this process are addressed in
439 the Discussion.
440
441 In the retina of aardvark 1, photoreceptor densities (and hence rod densities) were estimated
442 from counts of ONL nuclei in DAPI-stained vertical sections at 16 positions from the visual
443 streak region, midperipheral and peripheral retina. The observed range was about 124,000 –

444 214,000 photoreceptors (rods)/mm², with densities decreasing from central to peripheral
445 retina. In the retina of aardvark 2, photoreceptor densities were estimated from counts of ONL
446 somata at seven positions in vertical paraffin sections from central and midperipheral retina.
447 Here the range was about 182,000 – 245,000 photoreceptors (rods)/mm². The ONL had five to
448 nine tiers of photoreceptor somata like the ONL of aardvark 1. It is possible that aardvark 2
449 had higher rod densities than aardvark 1, but the larger shrinkage of paraffin-embedded tissue
450 may also have artefactually increased the cell density.
451
452 *Cone photoreceptors*
453 The cone photoreceptors were identified by labelling with antisera to the longwave-sensitive
454 (L) cone opsin and the shortwave-sensitive (S) cone opsin in retinal sections (Fig 6A, B) and
455 in flat-mounted retinal pieces from various retinal regions (Fig 6C, S1 Fig, S2 Fig). The two S
456 opsin antisera sc14363 (directed against an N-terminus epitope) and JH455 (directed against a
457 C-terminus epitope) showed complete colocalization of labelling (not illustrated). This is
458 evidence that a full-length, functional S opsin is present. Interestingly, a very large proportion
459 of aardvark cones throughout the retina showed co-expression of the L and S opsin.
460
461 **Fig 6. Cone photoreceptors** (aardvark 1). (**A, B**) Vertical retinal sections double-
462 immunolabelled for S cone opsin (A1, B1, red) and L cone opsin (A2, B2, green). In the
463 merged images, DAPI counterstaining in blue shows the retinal nuclear layers (A3, B3). Most
464 cones co-express S and L opsin, arrowheads point to pure S cones. In many cones of the
465 region shown in (A), both the S opsin and the L opsin label extend throughout the cone from
466 the OS to the cone pedicle in the OPL; in the region shown in (B), the L opsin label is
467 restricted to the OS. (**C**) Double immunolabelled cones in a flat-mounted piece from ventral
468 midperipheral retina. S opsin label (C1, magenta) and L opsin label (C2, green) are
469 colocalized in most cones (C3). Three of the pure S cones are indicated by arrowheads, pure L

470 cones are not present in this field. The aureole seen around most cones is an artefact; as the
471 cones were photographed from the vitreous side of the retina, there is light scatter at many
472 cellular structures. (**D**) Vertical section double-immunolabelled for S opsin (D1, in red,
473 showing the S cone pedicles in the OPL) and the synaptic ribbon marker CtBP2 (D2, in
474 green). Most of the small CtBP2 structures in the OPL are ribbons of rod spherules; the merge
475 (D3) shows that cone pedicles do not have the ribbon/CtBP2 clusters seen in other mammals.
476 As expected, many somata in the INL are also CtBP2-labelled. (**E**) Flat-mounted retinal piece
477 double-labelled for S opsin (E1, magenta) and CtBP2 (E2, green). The focus is on the cone
478 pedicles in the OPL. The merge (E3) confirms the absence of cone-typical ribbon/CtBP2
479 clusters at the pedicle. (A-E) are maximum intensity projections of confocal image stacks.
480 The stack in (C) starts at the level of the intensely labelled cone outer segments and ends at
481 the cone soma level. In this region, faint S opsin label extended throughout the cone, whereas
482 L opsin label was restricted to the outer segment in most of the cones. The stack in (E) is of 3
483 focal images spaced 0.5 µm apart. For layer abbreviations, see Fig. 3. Scale bar in (B3) is 100
484 µm and applies to (A, B); scale bar in (C3) is 50 µm; scale bars in (D3) and (E3) are 20 µm.
485
486 In sample fields across the retina of aardvark 1, between 35% and 96% were such dual
487 pigment cones. A substantial proportion of the cones were pure S cones without L opsin
488 expression (some marked in Fig 6A-C). In dorsal retina, between 2% and 37% of the cones
489 were pure S cones, in ventral retina, this percentage was between 22% and 65%. Hence, it
490 appears that the proportion of pure S cones is markedly higher in ventral than dorsal retina,
491 but the large variation of percentages between sampling fields also indicates a high local
492 variability. Only a small proportion of the cones were pure L cones without S opsin
493 expression. In many counting fields containing between 100 and 300 cones, pure L cones
494 were absent; in other fields, pure L cones comprised 0.3% to 7% of the cones with no obvious
495 regional trend.

496

497 In the retina of aardvark 2, the proportions were somewhat different. In several counting
498 fields from a sample region in far peripheral retina, 67-80% of the cones were co-expressing
499 L and S opsin, 15-21% were pure L cones, and 6-12% were pure S cones. In another region
500 from an unknown but probably also relatively peripheral location, 86-95% of the cones were
501 co-expressing L and S opsin, 2-6% were pure L cones, and 3-8% were pure S cones (S1 Fig).
502

503 These percentages have to be considered with some reservation. First, the relative intensity of
504 the L and S opsin label varied considerably between cones, in some cones one of the labels
505 was barely above background. This was particularly obvious in aardvark 2 (S1 Fig) but can
506 also be seen in aardvark 1 (Fig 6C). Hence, assessment of opsin co-expression has a
507 subjective component. Second, in many retinal regions, the L opsin label was restricted to the
508 cone outer segments (Fig 6B), whereas the S opsin label typically extended throughout the
509 cone including the soma, axon, and cone pedicle (Fig 6A, B, D, E). The cone opsin labelling
510 revealed some degree of post mortem outer segment damage, some outer segments were
511 elongated, others were just small stumps (see Fig 6C). Hence, S opsin-labelled cones could be
512 identified rather reliably by focusing through the outer retina to their soma level, whereas L
513 opsin expression may have been missed in cases of outer segment loss. Nevertheless, there
514 were many sampling fields where the cone outer segments were partially preserved, so the
515 above proportions of pure S and L cones are at least semi-quantitatively reliable.
516

517 The synaptic ribbon marker CtBP2 mainly revealed the single synaptic ribbons of rod
518 synaptic endings (rod spherules) in the OPL (Fig 6D, E). These synaptic ribbons often showed
519 the horseshoe shape that is typical for mammalian rod ribbons (Fig 6E2). In contrast to the
520 situation in other mammals, CtBP2 did not show the typical clustering of ribbons in the cone

521 pedicles; there were only a few or no CtBP2 puncta at the pedicles of S cones. This is
522 addressed in the Discussion.
523
524 The general cone marker peanut agglutinin (PNA) labelled the S cone pedicles in the aardvark
525 retina (S2 Fig). This was evident by the overlapping label of the pedicles by the S opsin
526 antiserum and PNA. The lateral displacement of the pedicles against the cone outer segments
527 (S2C Fig) is mostly due to slight tissue shearing during the mounting of the retinal pieces and
528 could be followed by tracing the stained S cone axons through the ONL in the image stacks.
529 The PNA label of cone pedicles varied in intensity and size; in a few S cone pedicles it was
530 absent or too faint to be detected. Surprisingly, the L cone pedicles did not show PNA
531 labelling. This was checked in several L cones found in appropriately stained retinal pieces.
532 Two pure L cones are present in the field shown in S2 Fig. It remains open whether PNA does
533 not label the L cone pedicles at all, or whether the label is below the detection threshold of our
534 staining.
535
536 For aardvark 1, cone densities were assessed in more than 70 sample fields in flat-mounted
537 pieces coming from various positions across central and peripheral retina. The sampled tissue
538 included a large piece of temporal retina that contained the presumed area centralis. Total
539 cone densities, i.e., of S cones, L cones and dual pigment cones, showed no strong central-
540 peripheral gradient. Highest densities of up to 1,100 – 1,300 cones/mm² were present in a
541 region about 4 mm temporal to the optic disc. Density minima of about 300 cones/mm² were
542 present in a few fields in dorsal peripheral retina, but many other fields in dorsal, ventral, and
543 nasal periphery had densities of 400 to 1,100 cones/mm². In pieces from midperipheral retina,
544 densities ranged from 600 to 1,000 cones/mm². In the region of the bright (unpigmented)
545 horizontal fundus band described above (see Fig 2C), the cone density did not increase, fields
546 from a temporal and a nasal region of the band had 600 – 900 cones/mm². This suggests that

547 the band does not represent a retinal specialization (visual streak) at the level of the cone
548 population. With rod densities of up to 214,000/mm² in central and down to 124,000/mm² in
549 peripheral retina, the above cone densities correspond to cone percentages of 0.25 – 0.85%
550 among the photoreceptors, with a rough average of approximately 0.5% cones over most of
551 the retina. For aardvark 2, total cone densities could only be determined in the two small
552 peripheral pieces of retina described above. They ranged from 1,100 to 1,600 cones/mm².
553 These densities are somewhat higher than those of aardvark 1. With the higher rod densities
554 of 182,000 – 245,000/mm², this again amounts to cone percentages of 0.5 – 0.9% of the
555 photoreceptors.
556
557 *Thyroid hormone levels*
558 Given the high incidence of cone opsin co-expression in the aardvark and the important role
559 of thyroid hormone (TH) in regulating cone spectral identity, we looked at the serum TH
560 levels available for aardvark 1 (five measurements within 2.5 years) and his adult son
561 aardvark 3 (one measurement) in comparison to published serum TH levels in some
562 representative mammals (Table 2). To our knowledge, these are the first published serum TH
563 levels for aardvarks. The serum values of total thyroxine (tT4), total triiodothyronine (tT3),
564 free T4 (fT4) and the biologically active form free T3 (fT3) are very similar for aardvark 1
565 and his son, and are also similar to or higher than the respective values in other mammals.
566 This suggests that aardvarks are not hypothyroid and that the S opsin dominance is not related
567 to a lack of TH (see Discussion).
568
569 **Table 2. Thyroid hormone serum levels in different mammals**
570 (Different units in the publications have been converted to unify the table)

Species / Animal	**tT4** (µg/dl)	**tT3** (ng/dl)	**fT4** (ng/dl)	**fT3** (pg/ml)	**TSH** (ng/ml)
Aardvark 1[1]	12 – >15	226.3 – 390.4	1.54 – 1.93	2.28 – 4.23	<0.03
Aardvark 3[1]	>15	304.2	2.25	3.32	nd

Asian elephant[2]	11.12	126.72	0.87	1.39	0.97
African elephant[2]	10.76	123.27	0.93	1.41	0.56
Manatee[3]	4.5 – 8.3	140 – 160	1.3 – 1.6	nd	nd
Cow[4]	3.9 – 8.8	70 – 250	1.3 – 2.4	2.3 – 7.8	nd
Dog[5,6]	1.5 – 1.6 (1.53 – 2.25)	76 – 84 (nd)	~1.75 (0.98 – 1.57)	~1.15 (nd)	nd (0.07 – 0.26)
Human[7]	5 – 12	80 – 220	0.7 – 1.9l	2.3 – 4.1	0.006 – 0.06

tT4 = total thyroxine T4, tT3 = total triiodothyronine T3, fT4 = free T4, fT3 = free T3; TSH = Thyroid-stimulating hormone, thyrotropin; nd = not determined.
[1]Frankfurt Zoo animals (see Methods); [2]Ref. [88]; [3]Ref. [89]; [4]Ref. [90]; [5]Ref. [91]; [6]Ref. [92]; [7]UCLA Health Website (https://www.uclahealth.org/medical-services/surgery/endocrine-surgery/conditions-treated/thyroid/normal-thyroid-hormone-levels), fT3 level from Cleveland Clinic (https://my.clevelandclinic.org/health/diagnostics/22425-triiodothyronine-t3)

Discussion

The aardvark's designation as a 'living fossil' [2] suggests that its eye and retina also may show prototypic, primordial mammalian features. On the other hand, the aardvark ancestor could already have been specialized on feeding on ants and termites, which speaks against a 'basic general' mammal. Hence, we were interested to study the aardvark's eye and retina when the opportunity arose. Early mammals are assumed to have gone through a 'nocturnal bottleneck' with associated adaptations to low-light vision (see, e.g., [23-27]). Most extant nocturnal mammals possess eye and retina features reflecting such an evolutionary adaptation: The eye optics with a proportionately large lens and cornea serves increased light capture. The retina has a dominance of the more light-sensitive rod photoreceptors and only a small minority of cone photoreceptors (review: [5]). The features of the aardvark eye and retina fit this 'nocturnal' category.

Until 2022, the only detailed study available on the aardvark eye and retina was by Victor Franz, dating back to 1909 [3]. It claimed a pure rod retina without cones, but concedes that the tissue conservation may not have been sufficient to prove the absence of cones. The absence of cones has since been repeated in various printed summaries and websites on

aardvark biology and vision ([28] page 326, [29] page 579, [1,30,31]; website examples: [32,33]). Franz [3] also claimed the absence of a tapetum lucidum, but conceded in a later handbook chapter that a tapetum lucidum fibrosum may be present ([34] page 1214). Recently, Paszta and colleagues published a study on general features of the aardvark eye and extraocular structures that included a brief description of the retina [9]. This paper similarly claimed an absence of cones, but reported a tapetum lucidum. Walls [23] also listed the aardvark as having 'eye shine' and a trace of a tapetum fibrosum (his Table VII, p. 241). The present study has assessed these claims.

The external dimensions of the eye of aardvark 1 are similar to those reported previously [3,9]. The corneal size and lens are large compared to total eye size, the ratios of corneal diameter to eye equatorial diameter (0.75), of corneal diameter to eye axial length (0.81), of lens diameter to eye equatorial diameter (0.58), and of lens thickness to eye axial length (0.45) are within the range seen across nocturnal mammals [25,35]. However, these parameters overlap between nocturnal, cathemeral/crepuscular, and diurnal mammals, so their diagnostic value is limited (for discussion see, e.g., [25], but also [36]).

Tapetum lucidum

Some nocturnal, crepuscular, and arrhythmic mammals have a reflective choroidal tapetum lucidum behind the retina to increase the amount of light absorbed by the photoreceptors. To observers the tapetal reflection appears as 'eye shine.' Morphologically, the two most common tapetum types are a 'tapetum cellulosum' where the reflecting structures termed rodlets are located intracellularly (found in Carnivora), and a 'tapetum fibrosum' where the reflecting structures termed fibrils are located extracellularly (found in Artiodactyla, Cetacea and Perissodactyla) (reviews: [37-39]). Our own observation (Fig 1) as well as images and a video in the internet (https://www.youtube.com/watch?v=apNr2HSrx6s), last accessed on

October 17, 2024; aardvark shown from minute 2:11) indicate that the aardvark may have a tapetum lucidum. Hence, it is surprising that Franz [3], Matas et al. [40] and Freeman et al. [41] describe the absence of a tapetum in the aardvark eye. In contrast, Walls [23] and Paszta et al. [9] describe the presence of a tapetum, which they consider to be a choroidal tapetum fibrosum.

Our more detailed histological observations confirm a choroidal tapetum. The ultrastructural appearance of the tapetal fibrils with their cross-striation (Fig 3C) indicates that the fibrils consist of collagen, which is typical for a tapetum fibrosum [38,42]. On the other hand, in cross-section, the aardvark tapetal fibrils show a substructure with concentric zones of different electron-density (Fig 3D). This is reminiscent of the substructure of the zinc-containing rodlets of the tapetum cellulosum in ferret and dog [43,44]. As our tissue fixation was not optimized for electron microscopy, the substructure of the aardvark tapetal fibrils may be an artefact. Unfortunately, our material did not allow us to determine whether the domains with their changing fibril orientations are contained intracellularly (suggesting a tapetum cellulosum) or whether they are extracellular (suggesting a tapetum fibrosum). Weighing all evidence, we think that the aardvark tapetum lucidum is of the fibrosum type. It would certainly seem unlikely that the aardvark has a mix of both tapetum types. In mammals with a tapetum lucidum (whether of the cellulosum or fibrosum type), the RPE cells in front of the tapetum are unpigmented or only minimally pigmented, such that the tapetum can in fact function as a reflector (reviews: [23] page 232; [38]). This is also the case in the aardvark.

Across mammals, the optically relevant properties of tapetum fibrosum fibrils and tapetum cellulosum rodlets are similar. Both have diameters of about 100-200 nm and are nearly hexagonally arranged with a spacing of about one fibril/rodlet diameter, suitable for constructive interference (e.g., sheep: [42]; bovine: [45]; cat: [46,47]; overviews: [38,39,48]).

649 The aardvark fibrils have comparable dimensions, but their spacing is more disordered. In
650 many domains they are loosely spaced and do not show a tight hexagonal arrangement. Also,
651 the aardvark tapetum layer is relatively thin and the tapetum lamination is not as conspicuous
652 as in other species. Overall, the aardvark appears to have a rudimentary version of a tapetum
653 lucidum. Nevertheless, it obviously shows the typical 'eye shine.'
654
655 *Avascular retina*
656 The aardvark retina is avascular, as observed by Franz [3] and Matas et al. [40], and
657 confirmed here. This also explains why we did not see any GFAP-labelled astrocytes. Retinal
658 astrocytes are neuroglia cells restricted to the optic nerve fibre layer and associated with blood
659 vessels as well as with retinal ganglion cell axons. In species with limited retinal
660 vascularization, they only occur in the vascularized regions, and in avascular retinae they are
661 completely absent (review: [17]). Avascular retinae have been found in several mammals
662 from different orders [23,49-52]. There is no convincing common explanation for why the
663 retinae of some species are avascular whereas those of most other species are vascularized to
664 various extents. Damsgaard and Country [52] conclude from their large data survey that the
665 ancestral mammal had an avascular retina, and that retinal vascularization was dynamically
666 gained and lost throughout subsequent mammalian evolution depending on species-specific
667 visual needs for retinal processing capacity, neuron numbers and hence retinal thickness.
668 Mammalian avascular retinae are generally thinner than vascularized ones, commonly below
669 150 µm (reviews: [51,52]). The reason is that they have to be supplied with oxygen by
670 diffusion from the choroidal capillary network, and the maximum oxygen diffusion distance
671 has been modeled to be about 143 µm [53], although this value has been questioned by some
672 authors [54]. At 120-180 µm, the aardvark retina is slightly thicker than other avascular
673 retinae, but it is still thinner than many vascular nocturnal retinae, particularly having a
674 thinner ONL and lower photoreceptor density (see below).

675

676 Chase [51] also stated that mammals with avascular retinae lack a tapetum lucidum and
677 assumed that this is because a tapetum would add to the tissue thickness that has to be reached
678 by choroidal oxygen. The aardvark tapetum lucidum is not in line with that assumption. The
679 elephants, the horse and the zebra are further examples of species with a tapetum lucidum and
680 an avascular retina [49,50]. In fact, the choriocapillaris, the actual release site of oxygen and
681 nutrients to the retina, is located in front of the choroidal tapetum, directly facing the RPE and
682 retina. Figure 3E-H shows this for the aardvark and elephant. The aardvark choriocapillaris
683 forms a very dense capillary mesh (Fig 3I) that obviously suffices to adequately supply the
684 retina. We conclude that Chase's assumption of an incompatibility of a (choroidal) tapetum
685 lucidum with an avascular retina is not tenable.

686

687 *Rods*

688 Typically for a nocturnal mammal, the vast majority of the aardvark photoreceptors are rods;
689 the proportion of only around 0.5% cones is low even among nocturnal species (review: [5]).
690 However, the estimated rod densities of 124,000 – 214,000/mm² for aardvark 1 and of
691 182,000 – 245,000/mm² for aardvark 2 are rather low in comparison to those of many other
692 nocturnal mammals, which may range from 200,000 rods/mm² to more than 700,000
693 rods/mm² [5]. These low rod densities and the correspondingly thinner ONL most likely are
694 correlated with the avascularity of the aardvark retina. The nocturnal Microchiroptera also
695 have avascular retinae (review: [51]), and rod densities in the greater horseshoe bat average
696 about 370,000 rods/mm², complemented by about 2.5% cones [55]. The avascular retina of
697 the nocturnal to crepuscular rabbit has between 300,000 rods/mm² in central and 130,00
698 rods/mm² in peripheral retina, complemented by about 4 – 6% cones [56]. Hence, even among
699 nocturnal mammals with avascular retinae, the aardvark rod density is in the lower range,
700 suggesting a low adaptive pressure for good nocturnal vision.

701

702 Also typical for nocturnal mammals is an inverted architecture of the rod nuclei [20]. Franz
703 [3] noted the central clustering of heterochromatin in the aardvark rods and described it as
704 'nuclei with two opposing chromatin bodies that looked like being in mitosis.' We here give a
705 detailed description of these rod nuclei (Fig 4). As analyzed by Solovei and colleagues
706 [20,22], the central position of the inactive heterochromatin and peripheral position of the
707 active euchromatin are assumed to be strongly disadvantageous for nuclear functions, but they
708 have an optical advantage. The densely packed heterochromatin core is highly refractive and
709 shows the physical properties of a light-focusing lens. Hence, the rod nuclei in the ONL form
710 columns of microlenses that act as 'light guides.' This strongly reduces light scattering in the
711 ONL, which is particularly important for nocturnal mammals with their thicker ONL and the
712 need to capture a large proportion of the few photons available at night. Obviously, inverted
713 rod nuclei are an evolutionary adaptation to improve nocturnal vision. The rods of diurnal
714 mammals have a conventional nuclear architecture, because they do not have to maximize
715 photon capture.

716

717 The aardvark has semi-inverted rod nuclei. Most likely, these are less effective focusing
718 lenses than fully inverted rod nuclei. Both the relatively low rod density compared to other
719 nocturnal mammals and the semi-inverted rod nuclei support the assumption that for the
720 aardvark with its reliance on smell and hearing, there was no strong evolutionary pressure for
721 an optimally adapted nocturnal retina, and that its night vision sensitivity is lower than that of
722 many other nocturnal mammals.

723

724 In conventional nuclei, heterochromatin is tethered to the nuclear envelope by either lamin
725 A/C or the lamin B receptor (LBR); the inverted rod nuclei of nocturnal mammals are
726 characterized by the absence of both tethers [57]. The semi-inverted architecture of the

727 aardvark rod nuclei might be explained by expression of one of these proteins. We tested this
728 with antibodies to LBR and to lamin A/C. Whereas no aardvark retinal neurons showed LBR
729 immunoreactivity, all of them showed lamin A/C immunoreactivity. The lamin A/C antibody
730 clearly marked the rod's nuclear periphery, although admittedly weaker compared to the
731 nuclei of the INL and GCL. This is similar to the weak LBR expression in the semi-inverted
732 rod nuclei of, e.g., goat and cow [57].
733
734 *Cones*
735 From today's perspective, the claim that the aardvark retina completely lacks cones [3,9] was
736 based on histological approaches that are not suitable to detect sparse populations of cones.
737 The most reliable approach to identify cones is by immunolabelling them with antibodies to
738 cone opsins, which we have done in the present study. The immunolabelling showed the
739 presence of L and S opsin in a low-density population of aardvark cones.
740
741 The two common mammalian cone opsins are the L opsin (also termed LWS opsin, peak
742 sensitivity λ_{max} in the green to yellow part of the spectrum) and the S opsin type 1 (SWS1
743 opsin, λ_{max} in the blue, violet or UV part of the spectrum [58]. The opsin antisera used here
744 recognize all spectral variants of the respective opsins. Partial gene sequencing has identified
745 L and S opsin genes in the aardvark, and judging from the tuning-relevant amino acids, the
746 aardvark S opsin has been suggested to be UV-sensitive, and the L opsin to have its λ_{max} at
747 527-533 nm (Supplementary Table S5 in [7]). UV tuning is the ancestral tuning of the
748 vertebrate SWS1 opsin and has been maintained in a number of nocturnal mammals (reviews:
749 [59-61]). Our opsin immunolabelling gives evidence that the L and S opsins are indeed
750 expressed in aardvark cones, and provides information about the population density and
751 topographical distribution of the cones.
752

A less normal feature of the aardvark cones is, that many of them co-express the two opsins across the retina and are 'dual pigment' cones. An artefactual double-labelling due to cross-reactivity between the two opsin antisera can be excluded, because the tissue also shows pure L and S cones. Many nocturnal mammals have the two opsins in separate cone populations and thus the basis for dichromatic color vision. This is the canonical mammalian condition of being spectrally selective (reviews: [4,5,62]). Dual pigment cones were reported in the ventral retinae of the house mouse, guinea pig and rabbit [63,64]. Since then, opsin co-expression in all cones across the retina has been found in the pouched mouse *Saccostomus campestris* and the Siberian dwarf hamster *Phodopus sungorus* [65]. The molecular mechanisms responsible for the co-expression of both opsins in some cones and its suppression in other cones is only partly understood. During rat and gerbil retinal development, all cones first express S opsin, and prospective L cones then successively switch to L opsin expression with an intermediate phase of opsin co-expression; this suggests that S opsin expression may be the default pathway when an L opsin-activating mechanism is absent or suppressed [66]. One such factor is thyroid hormone (see below).

In the retina of aardvark 1, the majority of single pigment cones are pure S cones (regionally varying from 2% to 65% of the cones); pure L cones are a sparse population of about 0.3 – 7%. In the peripheral retina of aardvark 2, there are somewhat more pure L cones (2 – 21%) than pure S cones (3 – 12%). If the aardvark has colour-processing (cone-opponent) retinal ganglion cells, most of their input will be from dual pigment cones. What they may be able to use for colour vision are the spectrally different sensitivities of pure L and S cones vs. dual pigment cones. The rods may also contribute to colour vision in mesopic light conditions ([58] and references therein). However, given the very low cone density and the dominance of dual pigment cones, it is likely that the aardvark at best has feeble colour vision [62]. The low cone density also makes good photopic visual acuity (cone-based spatial resolution) unlikely.

Our opsin immunolabelling showed qualitatively different mixtures of the two opsins in different cones, but did not allow to quantitatively access the absolute amounts of the two opsins per cone. Hence, we cannot comment on the presumed dominant spectral sensitivity of these dual-pigment cones. However, the much higher fraction of S opsin-containing cones in comparison to most other mammals suggests that the aardvark retina has a relatively high cone-based sensitivity in the shortwave (blue to UV) range. This is the case, e.g., in Microchiroptera with a similar S opsin dominance [67]. It may be an evolutionary adaptation to the spectral composition of twilight, which contains higher proportions of short wavelengths than full daylight (see, e.g., [68,69]). Twilight is the most likely situation that nocturnal animals may encounter during their active phases, and cones contribute to vision at this mesopic light level. On the other hand, many nocturnal mammals facing the same twilight conditions, e.g., rats [70], flying foxes [71], colugos [14], nocturnal lemurs [72], and Canidae [73], have low proportions of S cones (reviews: [4,5,60]). Moreover, a substantial number of nocturnal mammals are completely lacking S cones (review: [74]). That makes the hypothesis of a special shortwave adaptation to twilight less plausible.

As assessed in the retina of aardvark 1, cone density changes across the retina are small, ranging from a shallow maximum of up to 1,300 cones/mm² in a region of temporal retina to minima of 300 cones/mm² at some peripheral locations, but up to 1,100 cones/mm² in other peripheral regions, representing 0.25–0.85% of the photoreceptors. The horizontal band of reduced RPE pigmentation seen in the eye's fundus has no higher cone density than the surrounding midperiphery. Thus, the cone topography does not suggest specialized regions of particularly high cone-based visual performance like a prominent area centralis or visual streak. Such specialisations are present in many other mammals (reviews: [75-77]), but often most prominent in the retinal ganglion cells. The cone density in the small parts of the retina

805 of aardvark 2 that could be studied is slightly higher, but due to the higher rod densities there,
806 the cones also represent only 0.5–0.9% of the photoreceptors. Together with the different
807 proportions of pure L cones, pure S cones and dual pigment cones in the two individuals, it
808 appears that there is some interindividual variability in the detailed characteristics of the cone
809 population, even though the basic properties of a low cone-to-rod ratio and a dominance of
810 dual pigment cones are preserved. Alternatively, these differences between the old male
811 aardvark 1 and the younger female aardvark 2 could be sex-related or age-related. A larger
812 sample of aardvark retinae would be needed to study these aspects.
813
814 A further unusual feature of the aardvark cones is that the cone pedicles do not show the
815 typical cluster of CtBP2-positive ribbons. In other mammals, the cone pedicles have a large
816 number of presynaptic sites with ribbons (reviews: [78,79]). The tissue quality did not allow
817 an ultrastructural analysis, so we could not determine whether the aardvark cones have only
818 few ribbon synapses per pedicle, or whether there are many that do not label for CtBP2. A
819 low ribbon density may impair the signal transmission performance of the aardvark cones.
820
821 *Thyroid hormone (TH)*
822 In mouse early postnatal development, TH, through its receptor TRβ2, is a crucial regulator of
823 cone spectral identity by repressing S opsin and activating L opsin [80-82]. Even in adult
824 mouse and rat, pharmacological suppression of serum TH reversibly activates S opsin and
825 represses L opsin in all cones [83]. It may be that dual pigment cones are the consequence of a
826 (genetic) defect of the switch-off mechanism for S opsin expression during developmental L
827 opsin activation [84]. Hence, we were interested to know whether the aardvark has unusually
828 low TH levels that might correlate with the high proportion of dual pigment cones. The data
829 presented in Table 2 show that this is not the case, the aardvark has serum TH levels that are
830 similar to or higher than those of other mammals, particularly those of the elephants and the

manatee that belong to the same clade Afrotheria as the aardvark. The other listed species cover a broad range of mammals, and all of them have a normal cone complement with a majority of pure L cones and a ca. 10% minority of pure S cones (with the exception of the manatee, for which no cone population data exist). This suggests that aardvarks are not hypothyroid and that the S opsin dominance is not related to a lack of TH. Also, elevated serum levels of thyroid-stimulating hormone (TSH) would be a first sign of hypothyroidism, but they appear low in aardvark 1 (Table 2). However, there could be other deficits in the chain of thyroid hormone action that we were unable to study here. For example, one crucial component is the nuclear T3 receptor TRβ2; in TRβ2 knockout mice, all cones express S opsin and none express M opsin [80]. Another component is the monocarboxylate transporter 8 (MCT8), a plasma membrane transporter allowing TH access to the cones; in MCT8 knockout mice, cone opsin expression resembles that in hypothyroid or TRβ2 knockout mice [85].

Conclusions

The aardvark eye and retina have the typical features seen in nocturnal mammals: light-sensitive optics with a large lens and a large cornea, a reflective tapetum lucidum, and a rod dominance with a very low cone density. Three unusual features are, (i) that the retina is avascular with the corollary of being thinner and hence having a lower rod density than many other nocturnal mammals, (ii) that the rod nuclei are only semi-inverted and not fully inverted as in other nocturnal mammals, (iii) that there is opsin co-expression in a large proportion of the cones. Hence, nocturnal visual sensitivity probably is lower than in many other nocturnal mammals, and cone-based visual acuity and colour vision certainly are poor.

Regarding the designation of the aardvark as a living fossil [2] and the question whether this entails a primordial, prototypical mammalian retina, one can state that the massive presence of

dual pigment cones argues against a primordial character of the aardvark retina. The most common pattern in non-mammalian vertebrate retinae, as in mammalian retinae, are single opsin cones. The most parsimonious assumption is that the last synapsid ancestor of the mammals, and hence also the first mammal, had single opsin cones. Therefore, dual pigment cones are a derived feature, and the aardvark retina is not a primordial mammalian retina as far as the cones are concerned.

Acknowledgments

We thank Robert Molday and Jeremy Nathans for kindly providing antibodies. The technical assistance of Alena Konoplew, Elke Laedtke and Carola Tröger is gratefully acknowledged. We also thank Radosław Ratajszczak, Wojciech Paszta and Krzysztof Zagórski (Wrocław Zoo) for their help in collecting research material and for providing information on the animal from which the eyes were taken.

References

1. Shoshani J, Goldman CA, Thewissen JGM. *Orycteropus afer*. Mammalian Species. 1988; 300:1–8.
2. Shoshani J. Tubulidentata (Aardvarks). In: Encyclopedia of Life Sciences. John Wiley & Sons Ltd, Chichester; 2001. http://www.els.net. doi: 10.1038/npg.els.0001578.
3. Franz V. Das Auge von *Orycteropus afer* (Pallas). Denkschriften der medicinisch-naturwissenschaftlichen Gesellschaft zu Jena. 1909; 15:401–415, with plates XXV and XXVI.
4. Ahnelt PK, Kolb H. The mammalian photoreceptor mosaic: adaptative design. Progr Ret Eye Res. 2000; 19:711–777. doi: 10.1016/s1350-9462(00)00012-4.

883 5. Peichl L. Diversity of mammalian photoreceptor properties: Adaptations to habitat and
884 lifestyle? Anatomical Record, Part A, Discoveries in Molecular, Cellular, and
885 Evolutionary Biology. 2005; 287A:1001–1012. doi: 10.1002/ar.a.20262.
886 6. Meredith RW, Gatesy J, Emerling CA, York VM, Springer MS. Rod monochromacy
887 and the coevolution of cetacean retinal opsins. PLoS Genet. 2013; 9(4):e1003432. doi:
888 10.1371/journal.pgen.1003432.
889 7. Emerling CA, Springer MS. Eyes underground: Regression of visual protein networks
890 in subterranean mammals. Mol Phylogenet Evol. 2014; 78:260–270. doi:
891 10.1016/j.ympev.2014.05.016.
892 8. Emerling CA, Springer MS. Genomic evidence for rod monochromacy in sloths and
893 armadillos suggests early subterranean history for Xenarthra. Proc R Soc Lond. B.
894 2015; 282:20142192. doi: 10.1098/rspb.2014.2192.
895 9. Paszta W, Klećkowska-Nawrot JE, Goździewska-Harłajczuk K. Morphological
896 evaluation of the orbit, eye tunics, eyelids, and orbital glands in young and adult
897 aardvarks *Orycteropus afer*, Pallas, 1766 (Tubulidentata: Orycteropodidae):
898 Similarities and differences with representatives of the Afrotheria clade. Anat Rec.
899 2022; 305:3317–3340. doi: 10.1002/ar.24905.
900 10. Briggman KL, Helmstaedter M, Denk W. Wiring specificity in the direction-
901 selectivity circuit of the retina. Nature. 2011; 471:183–188. doi:10.1038/nature09818.
902 11. Tegethoff L, Briggman KL. Quantitative evaluation of embedding resins for volume
903 electron microscopy. Front Neurosci. 2024; 18:1286991. doi:
904 10.3389/fnins.2024.1286991.
905 12. Schiviz AN, Ruf T, Kuebber-Heiss A, Schubert C, Ahnelt PK. Retinal cone
906 topography of artiodactyl mammals: Influence of body height and habitat. J Comp
907 Neurol. 2008; 507(3):1336–1350. doi: 10.1002/cne.21626.

908 13. Schleich CE, Vielma A, Glösmann M, Palacios AG, Peichl L. Retinal photoreceptors
909 of two subterranean tuco-tuco species (Rodentia, *Ctenomys*): morphology, topography,
910 and spectral sensitivity. J Comp Neurol. 2010; 518:4001–4015. doi:
911 10.1002/cne.22440.
912 14. Moritz GL, Lim NT-L, Neitz M, Peichl L, Dominy NJ. Expression and evolution of
913 short wavelength sensitive opsins in colugos: A nocturnal lineage that informs debate
914 on primate origins. Evol Biol. 2013; 40:542–553. doi: 10.1007/s11692-013-9230-y.
915 15. Nießner C, Denzau S, Malkemper EP, Gross JC, Burda H, Winklhofer M, et al.
916 Cryptochrome 1 in retinal cone photoreceptors suggests a novel functional role in
917 mammals. Sci Rep. 2016; 6:21848. doi: 10.1038/srep21848.
918 16. Peichl L, Radic T, Solovei I, Wolfram M, Glösmann M. On the retinae of *Glis* and
919 *Graphiurus*: photoreceptor and ganglion cell populations, an absence of shortwave-
920 sensitive cones, and some other features (Rodentia: Gliridae). Lynx, n. s. (Praha).
921 2022; 53:185–205. doi: 10.37520/lynx.2022.013.
922 17. Schnitzer J. Astrocytes in mammalian retina. Progr Ret Res. 1988; 7:209–231.
923 18. Lewis GP, Fisher SK. Up-regulation of glial fibrillary acidic protein in response to
924 retinal injury: Its potential role in glial remodeling and a comparison to vimentin
925 expression. Int Rev Cytol. 2003; 230:263–290. doi: 10.1016/s0074-7696(03)30005-1.
926 19. Bringmann A, Iandiev I, Pannicke T, Wurm A, Hollborn M, Wiedemann P, et al.
927 Cellular signaling and factors involved in Müller cell gliosis: neuroprotective and
928 detrimental effects. Prog Ret Eye Res. 2009; 28:423–451. doi:
929 10.1016/j.preteyeres.2009.07.001.
930 20. Solovei I, Kreysing M, Lanctôt C, Kösem S, Peichl L, Cremer T, et al. Nuclear
931 architecture of rod photoreceptor cells adapts to vision in mammalian evolution. Cell.
932 2009; 137:356–368. doi: 10.1016/j.cell.2009.01.052.

933 21. Subramanian K, Weigert M, Borsch O, Petzold H, Garcia-Ulloa A, Myers EW, et al.
934 Rod nuclear architecture determines contrast transmission of the retina and behavioral
935 sensitivity in mice. eLife. 2019; 8:e49542. doi: 10.7554/eLife.49542.
936 22. Feodorova Y, Falk M, Mirny LA, Solovei I. Viewing nuclear architecture through the
937 eyes of nocturnal mammals. Trends Cell Biol. 2020; 30:276–289. doi:
938 10.1016/j.tcb.2019.12.008.
939 23. Walls GL. The Vertebrate Eye and its Adaptive Radiation. New York: Hafner
940 Publishing Company; 1942.
941 24. Heesy CP, Hall MI. The nocturnal bottleneck and the evolution of mammalian vision.
942 Brain Behav Evol. 2010; 75:195–203. doi: 10.1159/000314278.
943 25. Hall MI, Kamilar JM, Kirk EC. Eye shape and the nocturnal bottleneck of mammals.
944 Proc R Soc Lond B. 2012; 279:4962–4968. doi: 10.1098/rspb.2012.2258.
945 26. Gerkema MP, Davies WIL, Foster RG, Menaker M, Hut RA. The nocturnal bottleneck
946 and the evolution of activity patterns in mammals. Proc R Soc Lond B. 2013;
947 280:20130508. doi: 10.1098/rspb.2013.0508.
948 27. Maor R, Dayan T, Ferguson-Gow H, Jones KE. Temporal niche expansion in
949 mammals from a nocturnal ancestor after dinosaur extinction. Nature Ecology &
950 Evolution. 2017; 1:1889–1895. doi: 10.1038/s41559-017-0366-5.
951 28. Kolmer W. Die Netzhaut (Retina). In: v. Möllendorff W, editor. Handbuch der
952 mikroskopischen Anatomie des Menschen, Band 3, Teil 2 Auge. Berlin: Verlag Julius
953 Springer; 1936. pp. 295–468.
954 29. Rochon-Duvigneaud A. Les Yeux et la Vision des Vertébrés. Paris: Masson et Cie.;
955 1943.
956 30. Rahm U. Erdferkel oder Röhrchenzähner. In: Altevogt R, et al., editors. Grzimeks
957 Tierleben – Enzyklopädie des Tierreichs, 12. Band Säugetiere 3. Zürich: Kindler
958 Verlag; 1972. pp. 474–478.

31. Rahm U. Röhrchenzähner. In: Altevogt R, et al., editors. Grzimeks Enzyklopädie Säugetiere, Band 4. München: Kindler Verlag; 1987. pp. 452–458.
32. Ratzloff E. *Orycteropus afer* (Online). 2011. Available from: https://animaldiversity.org/accounts/Orycteropus_afer (last accessed October 17, 2024).
33. Klappenbach L. Aardvark fast facts (Online). 2019. Available from: https://www.thoughtco.com/aardvark-profile-129412 (last accessed October 23, 2024).
34. Franz V. Vergleichende Anatomie des Wirbeltierauges. In: Bolk L, Göppert E, Kallius E, Lubosch W, editors. Handbuch der vergleichenden Anatomie der Wirbeltiere, Vol. 2, Part 2 Sinnesorgane. Berlin and Vienna: Urban & Schwarzenberg; 1934. pp. 989–1292.
35. Kirk EC. Eye morphology in cathemeral lemurids and other mammals. Folia Primatol. (Basel) 2006; 77:27–49. doi: 10.1159/000089694.
36. Schmitz L, Motani R. Morphological differences between the eyeballs of nocturnal and diurnal amniotes revisited from optical perspectives of visual environments. Vis Res. 2010; 50:936–946. doi: 10.1016/j.visres.2010.03.009.
37. Schwab IR, Yuen CK, Buyukmihci NC, Blankenship TN, Fitzgerald PG. Evolution of the tapetum. Trans Am Ophthalmol Soc. 2002; 100:187–200.
38. Ollivier FJ, Samuelson DA, Brooks DE, Lewis PA, Kallberg ME, Komáromy AM. Comparative morphology of the tapetum lucidum (among selected species). Vet Ophthalmol. 2004; 7:11–22. doi: 10.1111/J.1463-5224.2004.00318.X.
39. Zueva L, Zayas-Santiago A, Rojas L, Sanabria P, Alves J, Tsytsarev V, et al. Multilayer subwavelength gratings or sandwiches with periodic structure shape light reflection in the *tapetum lucidum* of taxonomically diverse vertebrate animals. J Biophotonics. 2022; 15:e202200002. doi: 10.1002/jbio.202200002.

984 40. Matas M, Wise I, Masters NJ, Stewart J, Holloway A. Unilateral eyelid lesion and
985 ophthalmologic findings in an aardvark (*Orycteropus afer*): case report and literature
986 review. Vet Ophthalmol. 2010; 13 (suppl. 1):116–122. doi: 10.1111/j.1463-
987 5224.2010.00803.x.
988 41. Freeman K, Ben-Shlomo G, McMullen R, Moore BA. Ophthalmology of Afrotheria:
989 Aardvarks, Hyraxes, Elephants, Manatees, and Relatives. In: F. Montiani-Ferreira F,
990 Moore BA, Ben-Shlomo G, editors. Wild and Exotic Animal Ophthalmology, Vol. 2
991 Mammals. Springer Nature Switzerland; 2022. pp. 49–70.
992 42. Bellairs R, Harkness ML, Harkness RD. The structure of the tapetum of the eye of the
993 sheep. Cell Tissue Res. 1975; 157:73–91. doi: 10.1007/BF00223231.
994 43. Tjälve H, Frank A. Tapetum lucidum in the pigmented and albino ferret. Exp Eye Res.
995 1984; 38:341–351. doi: 10.1016/0014-4835(84)90189-1.
996 44. Wen GY, Sturman JA, Shek JW. A comparative study of the tapetum, retina and skull
997 of the ferret, dog and cat. Lab Anim Sci. 1985; 35(3):200–210. PMID: 4021435.
998 45. Braekevelt CR. Fine structure of the bovine tapetum fibrosum. Anat Histol Embryol.
999 1986; 15:215–222. doi: 10.1111/j.1439-0264.1986.tb00713.x.
1000 46. Bernstein MH, Pease DC. Electron microscopy of the tapetum lucidum of the cat. J
1001 Biophys Biochem Cytol. 1959; 5:35–40. doi: 10.1083/jcb.5.1.35.
1002 47. Braekevelt CR. Fine structure of the feline tapetum. Anat Histol Embryol. 1990;
1003 19:97–105. doi: 10.1111/j.1439-0264.1990.tb00892.x.
1004 48. Bortolami R, Callegari E, Lucchi ML. Ultrastructural observations on the tapetum
1005 lucidum fibrosum. Anat Histol Embryol. 1979; 8:72–78. doi: 10.1111/j.1439-
1006 0264.1979.tb00680.x.
1007 49. Johnson GL. Contributions to the comparative anatomy of the mammalian eye, chiefly
1008 based on ophthalmoscopic examination. Phil Trans R Soc Lond Series B. 1901;
1009 194:1–82.

1010 50. Johnson GL. Ophthalmoscopic studies on the eyes of mammals. Phil Trans R Soc
1011 Lond Series B. 1968; 254 (no. 794):207–220.
1012 51. Chase J. The evolution of retinal vascularization in mammals: a comparison of
1013 vascular and avascular retinae. Ophthalmology. 1982; 89:1518–1525. doi:
1014 10.1016/s0161-6420(82)34608-4.
1015 52. Damsgaard C, Country MW. The opto-respiratory compromise: balancing oxygen
1016 supply and light transmittance in the retina. Physiology. 2022; 37:101–113. doi:
1017 10.1152/physiol.00027.2021.
1018 53. Dollery CT, Bulpitt CJ, Kohner EM. Oxygen supply to the retina from the retinal and
1019 choroidal circulations at normal and increased arterial oxygen tensions. Invest
1020 Ophthalmol. 1969; 8:588–594. PMID: 5395349.
1021 54. Buttery RG, Hinrichsen CF, Weller WL, Haight JR. How thick should a retina be? A
1022 comparative study of mammalian species with and without intraretinal vasculature.
1023 Vision Res. 1991; 31:169–187. doi: 10.1016/0042-6989(91)90110-q.
1024 55. Kim T-J, Jeon Y-K, Lee J-Y, Lee E-S, Jeon C-J. The photoreceptor populations in the
1025 retina of the greater horseshoe bat *Rhinolophus ferrumequinum*. Mol Cells. 2008;
1026 26:373–379. doi: 10.1016/S1016-8478(23)14011-8.
1027 56. Young HM, Vaney DI. Rod-Signal interneurons in the rabbit retina: 1. rod bipolar
1028 cells. J Comp Neurol. 1991; 310:139–153. doi: 10.1002/cne.903100202.
1029 57. Solovei I, Wang AS, Thanisch K, Schmidt CS, Krebs S, Zwerger M, et al. LBR and
1030 lamin A/C sequentially tether peripheral heterochromatin and inversely regulate
1031 differentiation. Cell. 2013; 152:584–598. doi: 10.1016/j.cell.2013.01.009.
1032 58. Jacobs GH. Evolution of colour vision in mammals. Phil Trans R Soc Lond Series B.
1033 2009; 364:2957–2967. doi: 10.1098/rstb.2009.0039.

1034 59. Hunt DM, Carvalho LS, Cowing JA, Parry JW, Wilkie SE, Davies WL, et al. Spectral
1035 tuning of shortwave-sensitive visual pigments in vertebrates. Photochem Photobiol.
1036 2007; 83:303–310. doi: 10.1562/2006-06-27-IR-952.
1037 60. Hunt DM, Peichl L. S cones: Evolution, retinal distribution, development, and spectral
1038 sensitivity. Vis Neurosci. 2014; 31:115–138. doi:10.1017/S0952523813000242.
1039 61. Emerling CA, Huynh HT, Nguyen MA, Meredith RW, Springer MS. Spectral shifts of
1040 mammalian ultraviolet-sensitive pigments (short wavelength-sensitive opsin 1) are
1041 associated with eye length and photic niche evolution. Proc R Soc Lond B. 2015;
1042 282:20151817. doi: 10.1098/rspb.2015.1817.
1043 62. Jacobs GH. The distribution and nature of colour vision among the mammals. Biol
1044 Rev. 1993; 68:413–471. doi: 10.1111/j.1469-185x.1993.tb00738.x.
1045 63. Röhlich P, van Veen T, Szél Á. Two different visual pigments in one retinal cone cell.
1046 Neuron. 1994; 13:1159–1166. doi: 10.1016/0896-6273(94)90053-1.
1047 64. Applebury ML, Antoch MP, Baxter LC, Chun LL, Falk JD, Farhangfar F, et al. The
1048 murine cone photoreceptor: a single cone type expresses both S and M opsins with
1049 retinal spatial patterning. Neuron. 2000; 27:513–523. doi: 10.1016/s0896-
1050 6273(00)00062-3.
1051 65. Lukáts Á, Szabó A, Röhlich P, Vigh B, Szél Á. Photopigment coexpression in
1052 mammals: comparative and developmental aspects. Histol Histopathol. 2005; 20:551–
1053 574. doi: 10.14670/HH-20.551.
1054 66. Szél A, van Veen T, Röhlich P. Retinal cone differentiation. Nature. 1994; 370:336.
1055 doi: 10.1038/370336a0.
1056 67. Müller B, Glösmann M, Peichl L, Knop GC, Hagemann C, Ammermüller J. Bat eyes
1057 have ultraviolet-sensitive cone photoreceptors. PLoS ONE. 2009; 4(7):e6390). doi:
1058 10.1371/journal.pone.0006390.

1059 68. Roenneberg T, Merrow M. Light reception: discovering the clock-eye in mammals.
1060 Curr Biol. 2002; 12:R163–R165. doi: 10.1016/s0960-9822(02)00731-5.
1061 69. Walmsley L, Hanna L, Mouland J, Martial F, West A, Smedley AR, et al. Colour as a
1062 signal for entraining the mammalian circadian clock. PLoS Biol. 2015;
1063 13(4):e1002127. doi: 10.1371/journal.pbio.1002127.
1064 70. Szél A, Röhlich P. Two cone types of the rat retina detected by anti-visual pigment
1065 antibodies. Exp Eye Res. 1992; 55:47–52. doi: 10.1016/0014-4835(92)90090-f.
1066 71. Müller B, Goodman SM, Peichl L. Cone photoreceptor diversity in the retinas of fruit
1067 bats (Megachiroptera). Brain Behav Evol. 2007; 70:90–104. doi: 10.1159/000102971.
1068 72. Peichl L, Kaiser A, Rakotondraparany F, Dubielzig RR, Goodman SM, Kappeler PM.
1069 Diversity of photoreceptor arrangements in nocturnal, cathemeral and diurnal
1070 Malagasy lemurs. J Comp Neurol. 2019; 527(1):13–37. doi: 10.1002/cne.24167.
1071 73. Mowat FM, Peichl L. Ophthalmology of canidae: foxes, wolves, and relatives. In:
1072 Montiani-Ferreira F, Moore BA, Ben-Shlomo G, editors. Wild and Exotic Animal
1073 Ophthalmology, Vol. 2 Mammals. Springer Nature Switzerland; 2022. pp. 181–214.
1074 doi: 10.1007/978-3-030-81273-7_11.
1075 74. Jacobs GH. Losses of functional opsin genes, short-wavelength cone photopigments,
1076 and color vision—A significant trend in the evolution of mammalian vision. Vis
1077 Neurosci. 2013; 30:39–53. doi:10.1017/S0952523812000429.
1078 75. Hughes A. The topography of vision in mammals of contrasting life style: comparative
1079 optics and retinal organisation. In: Crescitelli F, editor. Handbook of Sensory
1080 Physiology, Vol. VII/5: The Visual System in Vertebrates. New York: Springer; 1977.
1081 pp. 613–756.
1082 76. Moore BA, Tyrrell LP, Kamilar JM, Collin SP, Dominy NJ, Hall MI, et al. Structure
1083 and function of regional specializations in the vertebrate retina. In: Kaas JH, editor.

1084 Evolution of Nervous Systems (2nd ed). Amsterdam: Elsevier; 2017. pp. 351–372.
1085 doi: 10.1016/B978-0-12-804042-3.00008-7.
1086 77. Heukamp AS, Warwick RA, Rivlin-Etzion M. Topographic variations in retinal
1087 encoding of visual space. Annu Rev Vis Sci. 2020; 6:237–259. doi: 10.1146/annurev-
1088 vision-121219-081831.
1089 78. tom Dieck S, Brandstätter JH. Ribbon synapses of the retina. Cell Tissue Res. 2006;
1090 326:339-346. doi: 10.1007/s00441-006-0234-0.
1091 79. Regus-Leidig H, Brandstätter JH. Structure and function of a complex sensory
1092 synapse. Acta Physiol. 2012; 204:479–486. doi: 10.1111/j.1748-1716.2011.02355.x.
1093 80. Ng L, Hurley JB, Dierks B, Srinivas M, Saltó C, Vennström B, et al. A thyroid
1094 hormone receptor that is required for the development of green cone photoreceptors.
1095 Nat Genet. 2001; 27:94–98. doi: 10.1038/83829.
1096 81. Roberts MR, Srinivas M, Forrest D, Morreale de Escobar G, Reh TA. Making the
1097 gradient: thyroid hormone regulates cone opsin expression in the developing mouse
1098 retina. Proc Natl Acad Sci U S A. 2006; 103:6218–6223. doi:
1099 10.1073/pnas.0509981103.
1100 82. Applebury ML, Farhangfar F, Glösmann M, Hashimoto K, Kage K, Robbins JT, et al.
1101 Transient expression of thyroid hormone nuclear receptor TRbeta2 sets S opsin
1102 patterning during cone photoreceptor genesis. Devel Dynamics. 2007; 236:1203–1212.
1103 doi: 10.1002/dvdy.21155.
1104 83. Glaschke A, Weiland J, Del Turco D, Steiner M, Peichl L, Glösmann M. Thyroid
1105 hormone controls cone opsin expression in the retina of adult rodents. J Neurosci.
1106 2011; 31:4844–4851. doi: 10.1523/JNEUROSCI.6181-10.2011.
1107 84. Neitz M, Neitz J. The uncommon retina of the common house mouse. Trends in
1108 Neurosciences. 2001; 24(5):248-249. doi: 10.1016/s0166-2236(00)01773-2.

1109 85. Liu Y, Ng L, Liu H, Heuer H, Forrest D. Cone photoreceptor differentiation regulated
1110 by thyroid hormone transporter MCT8 in the retinal pigment epithelium. Proc Natl
1111 Acad Sci U S A. 2024; 121:e2402560121. doi: 10.1073/pnas.2402560121.
1112 86. Hicks D, Molday RS. Differential immunogold-dextran labeling of bovine and frog
1113 rod and cone cells using monoclonal antibodies against bovine rhodopsin. Exp Eye
1114 Res. 1986; 42:55–71. doi: 10.1016/0014-4835(86)90017-5.
1115 87. Wang Y, Macke JP, Merbs SL, Zack DJ, Klaunberg B, Bennett J, et al. A locus
1116 control region adjacent to the human red and green visual pigment genes. Neuron.
1117 1992; 9:429–440. doi: 10.1016/0896-6273(92)90181-c. PMID: 1524826.
1118 88. Brown JL, Walker SL, Moeller T. Comparative endocrinology of cycling and non-
1119 cycling Asian (*Elephas maximus*) and African (*Loxodonta africana*) elephants. Gen
1120 Comp Endocr. 2004; 136:360–370. doi:10.1016/j.ygcen.2004.01.013.
1121 89. Ortiz RM, MacKenzie DS, Worthy GAJ. Thyroid hormone concentrations in captive
1122 and free-ranging West Indian manatees (*Trichechus manatus*). J Exp Biol. 2000;
1123 203:3631–3637. doi: 10.1242/jeb.203.23.3631.
1124 90. Nixon DA, Akasha MA, Anderson RR. Free and total thyroid hormones in serum of
1125 Holstein cows. J Dairy Sci. 1988; 71:1152–1160. doi: 10.3168/jds.S0022-
1126 0302(88)79669-1.
1127 91. Wahrendorf S. Schilddrüsenparameter und Cholesterol-Werte bei
1128 verhaltensunauffälligen Hunden. PhD Thesis, Faculty of Veterinary Medicine, Ludwig
1129 Maximilians University Munich; 2011. doi: 10.5282/edoc.12999. Available from:
1130 https://edoc.ub.uni-muenchen.de/12999/1/Wahrendorf_Silke.pdf
1131 92. Hegstad-Davies RL, Torres SMF, Sharkey LC, Gresch SC, Muñoz-Zanzi CA, Davies
1132 PR. Breed-specific reference intervals for assessing thyroid function in seven dog
1133 breeds. J Vet Diagn Invest. 2015; 27:716–727. doi: 10.1177/1040638715606953.
1134

1135

1136

1137 **Supporting information**

1138 **S1 Fig. Cone photoreceptors**. Sequentially double immunolabelled cones in two
1139 neighbouring flat-mounted pieces from an unknown location in midperipheral to peripheral
1140 retina (aardvark 2). The piece of field 1 was first incubated with the rabbit L opsin antiserum
1141 JH492, visualized with an Alexa488-coupled secondary antiserum (green). Then it was
1142 incubated with the rabbit S opsin antiserum JH455, visualized with a Cy3-coupled secondary
1143 antiserum (magenta). The merge shows that all cones are labelled by Cy3, because this
1144 secondary antiserum bound to JH455 as well as JH492. The pure S cones are exclusively
1145 labelled by Cy3 (arrowheads), all Alexa488-labelled cones contain the L opsin. The
1146 neighbouring piece of field 2 was first incubated with the rabbit S opsin antiserum JH455,
1147 visualized with the Cy3-coupled secondary antiserum (magenta). Then it was incubated with
1148 the rabbit L opsin antiserum JH492, visualized with the Alexa488-coupled secondary
1149 antiserum (green). The merge shows that all cones are labelled by Alexa488, because this
1150 secondary antiserum bound to JH492 as well as JH455. The pure L cones are exclusively
1151 labelled by Alexa488 (arrowheads), all Cy3-labelled cones contain the S opsin. The relative
1152 amount of L and S opsin (i.e., labelling intensity) differs between cones. For details of the
1153 procedure see Methods. The images are maximum intensity projections of confocal image
1154 stacks. Scale bar is 50 µm and applies to all images.

1155

1156 **S2 Fig. Cone photoreceptors and their synaptic pedicles in the outer plexiform layer.**
1157 Flat-mounted piece of retina (aardvark 1), triple immunolabelled for S opsin, L opsin and
1158 PNA. (**A**) Focus on the outer segments of the opsin-immunolabelled cones; most cones
1159 express both opsins (A1, S opsin; A2, L opsin; A3, merge). The field contains two pure L
1160 cones. (**B**) Focus on the cone pedicles in the outer plexiform layer; the S opsin-labelled

1161 pedicles (B1) are also labelled by PNA (B2), as shown in the merge (B3). (**C**) Schematic
1162 illustration of the cones identified in A (S cones, magenta circles; L cones, green circles; dual
1163 pigment cones, bipartite circles) and the PNA-labelled pedicles identified in B (grey squares).
1164 The pairing between outer segments and pedicles (connecting lines) was checked by
1165 following the S opsin-labelled cone axons through the image stacks. The pedicles of the two
1166 pure L cones show no PNA label. For two pedicles at the edges of the image, the
1167 corresponding outer segments lie outside the frame. Due to faint labelling of some cones, not
1168 all cones shown in (C) can be seen in (A) and (B). Scale bar in (C) is 50 µm and applies to all
1169 images.
1170

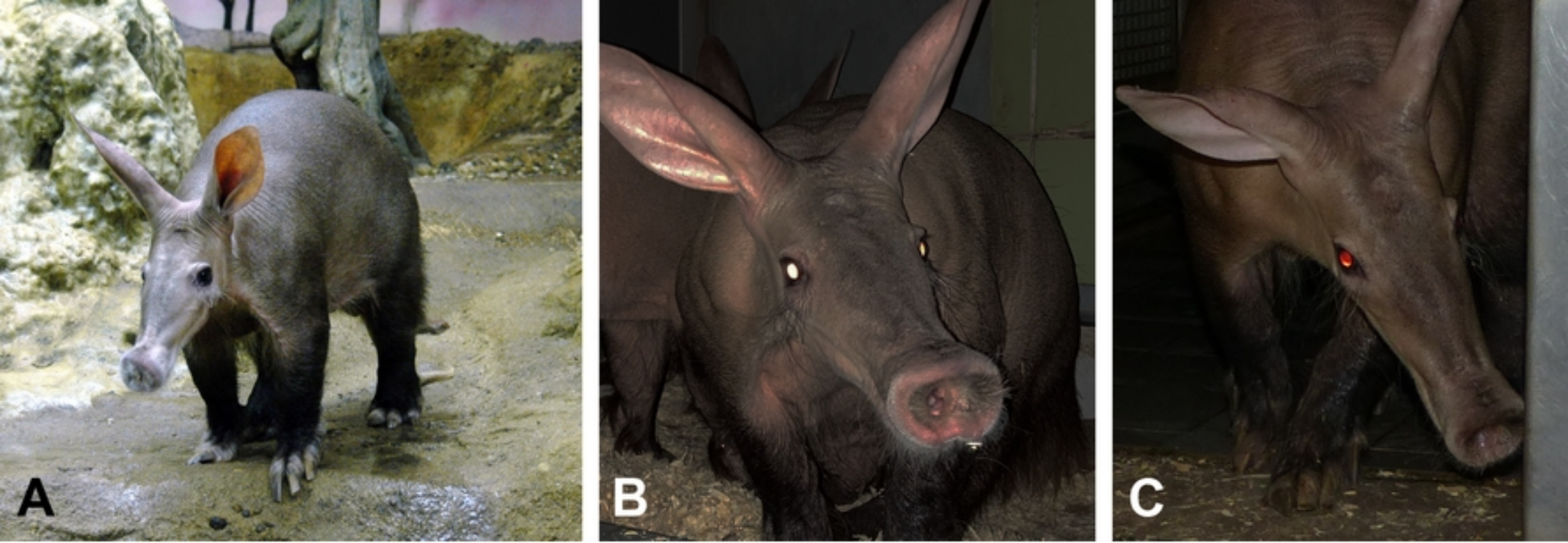

Figure 1

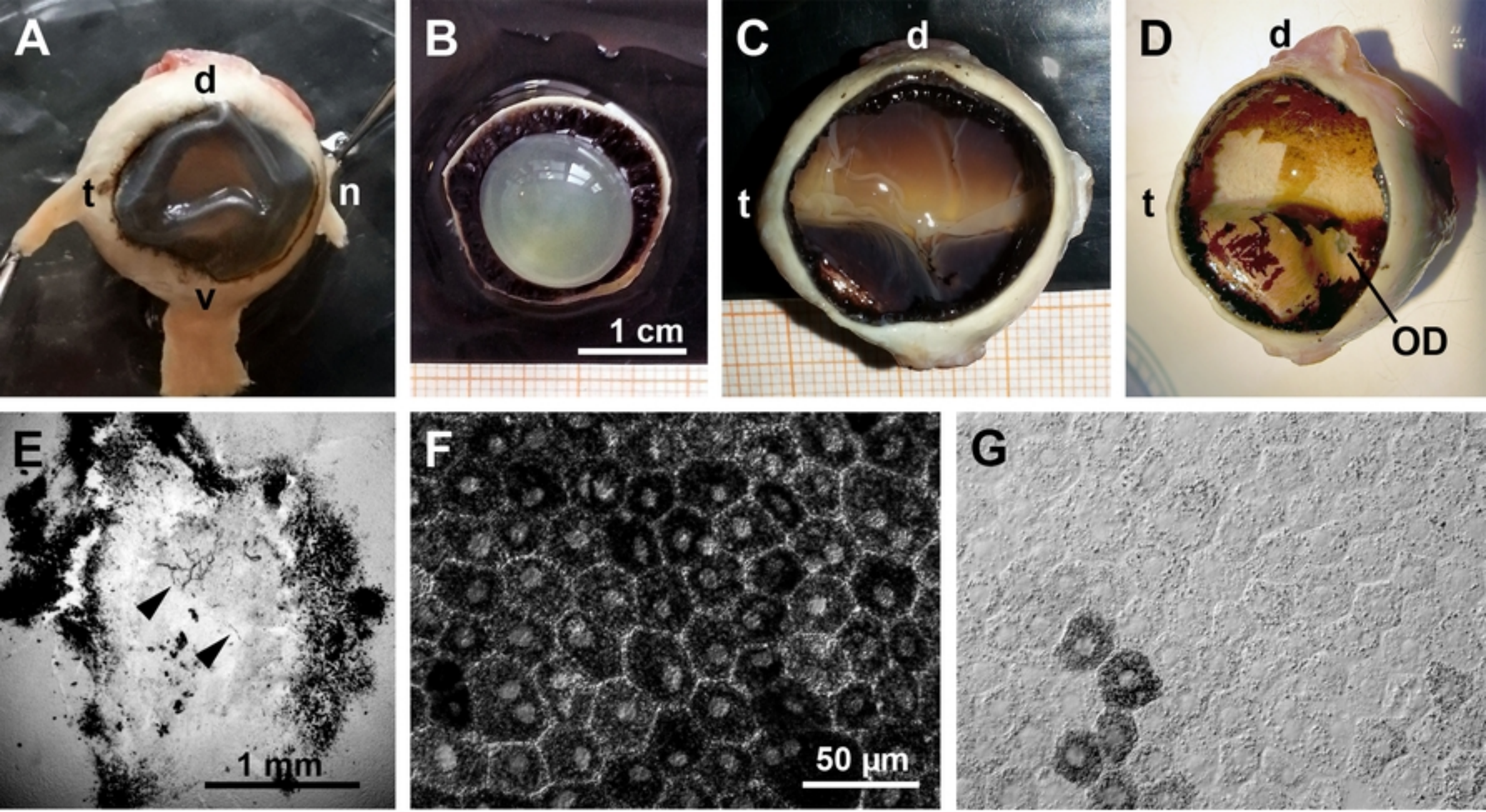

Figure 2

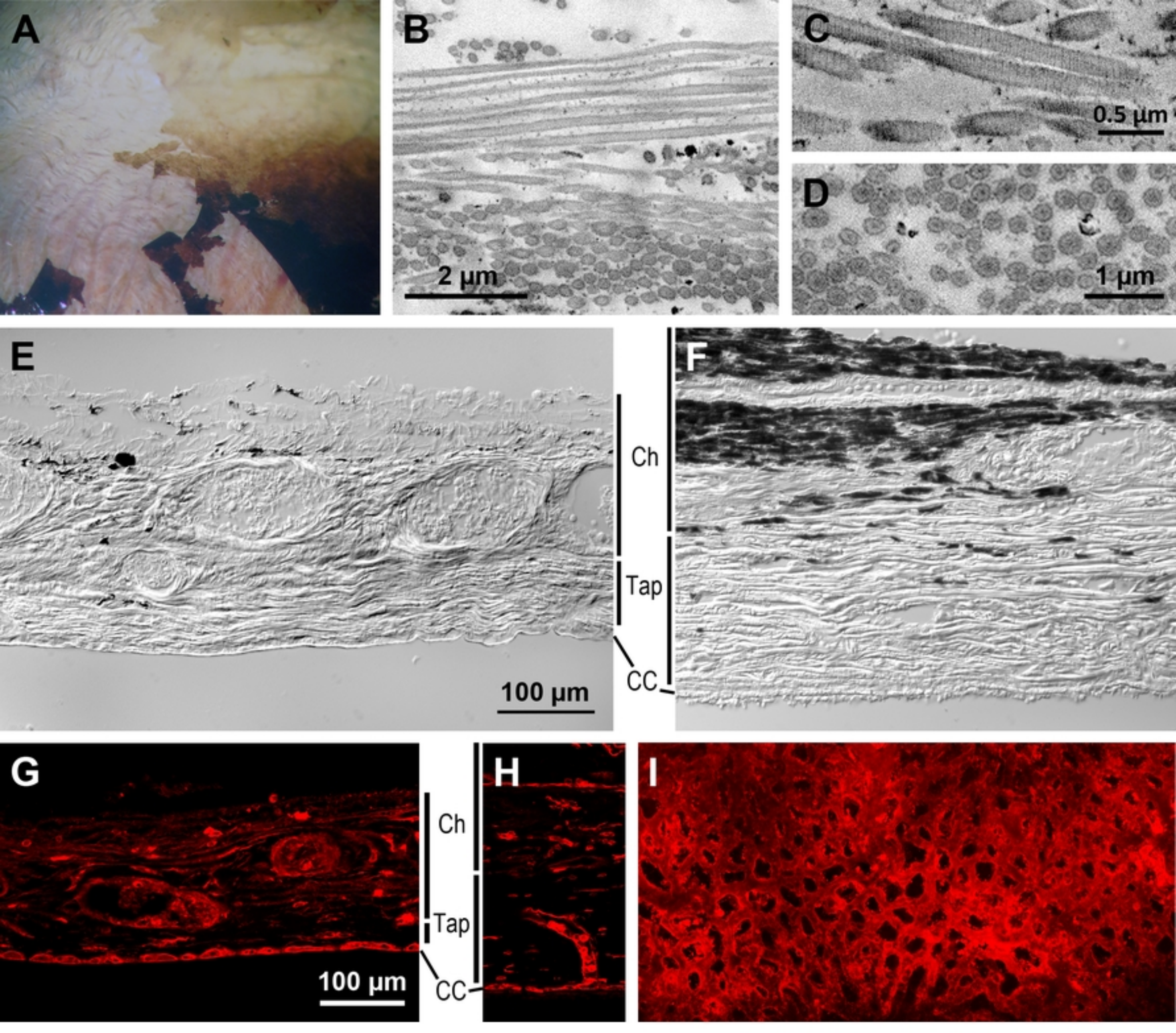

Figure 3

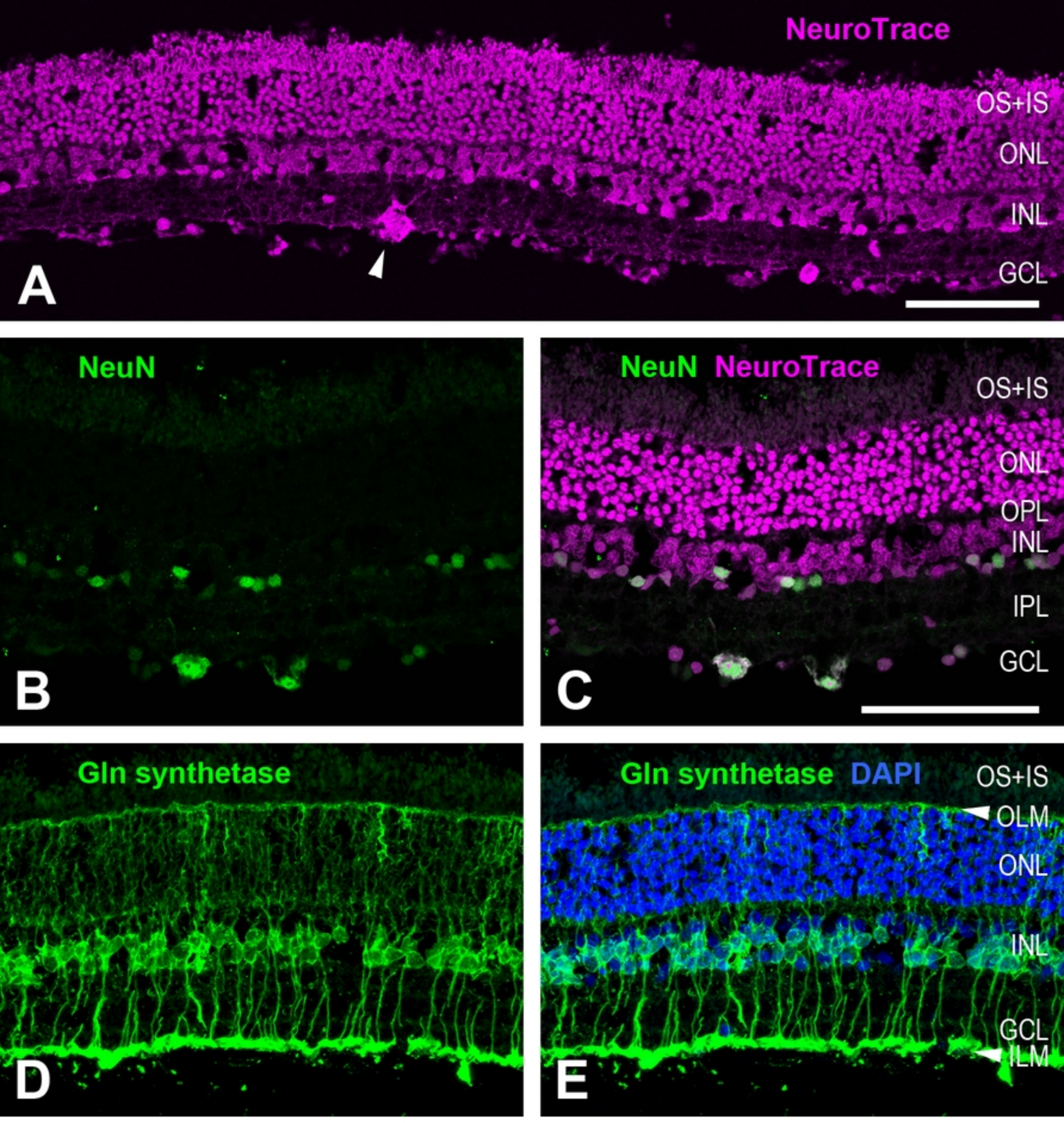
NeuroTrace
OS+IS
ONL
INL
GCL
A
NeuN
B
NeuN NeuroTrace
OS+IS
ONL
OPL
INL
IPL
GCL
C
Gln synthetase
D
Gln synthetase DAPI
OS+IS
OLM
ONL
INL
GCL
ILM
E

Figure 4

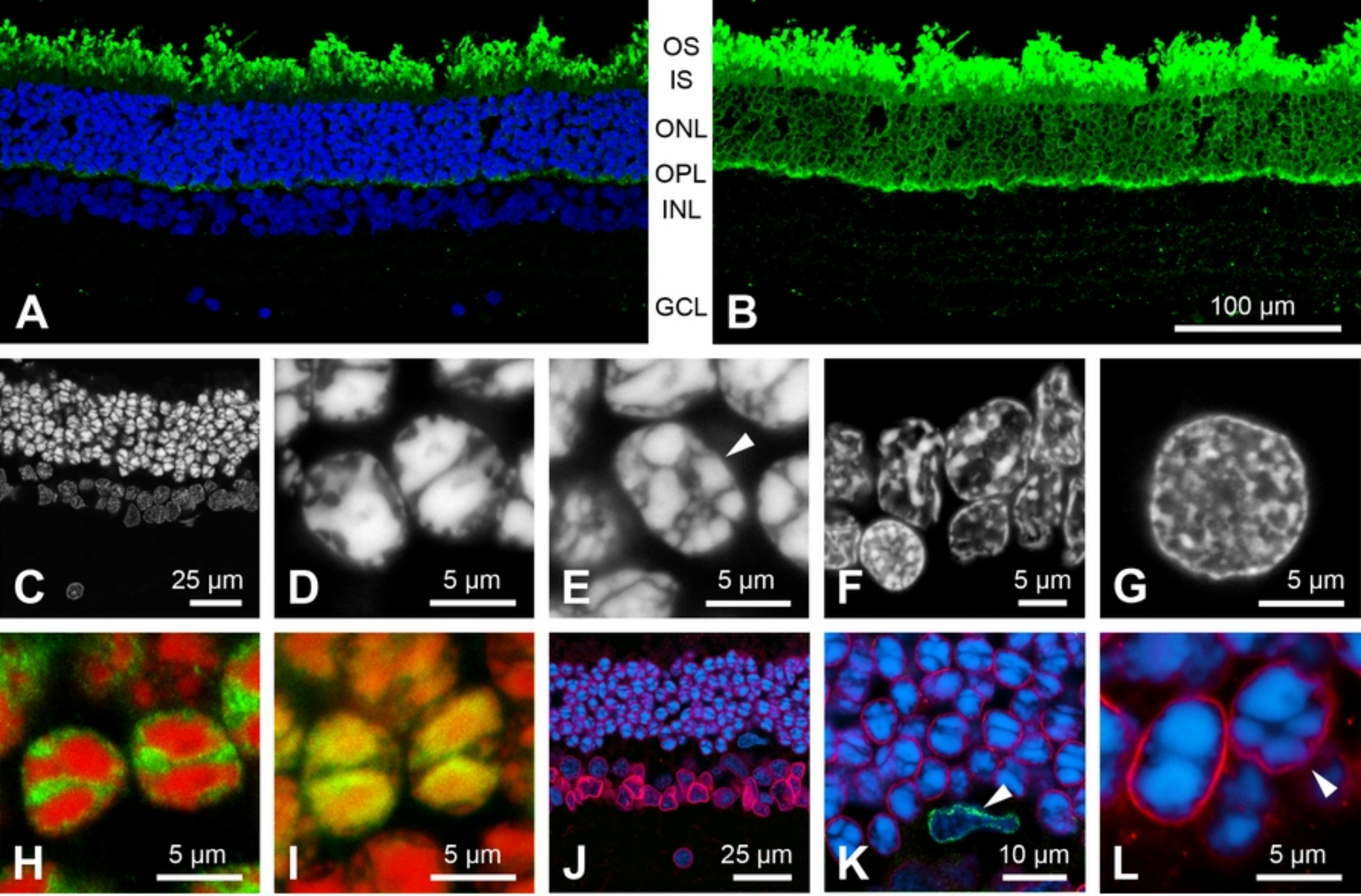
OS
IS
ONL
OPL
INL
GCL
A
B
100 µm
C
25 µm
D
5 µm
E
5 µm
F
5 µm
G
5 µm
H
5 µm
I
5 µm
J
25 µm
K
10 µm
L
5 µm

Figure 5

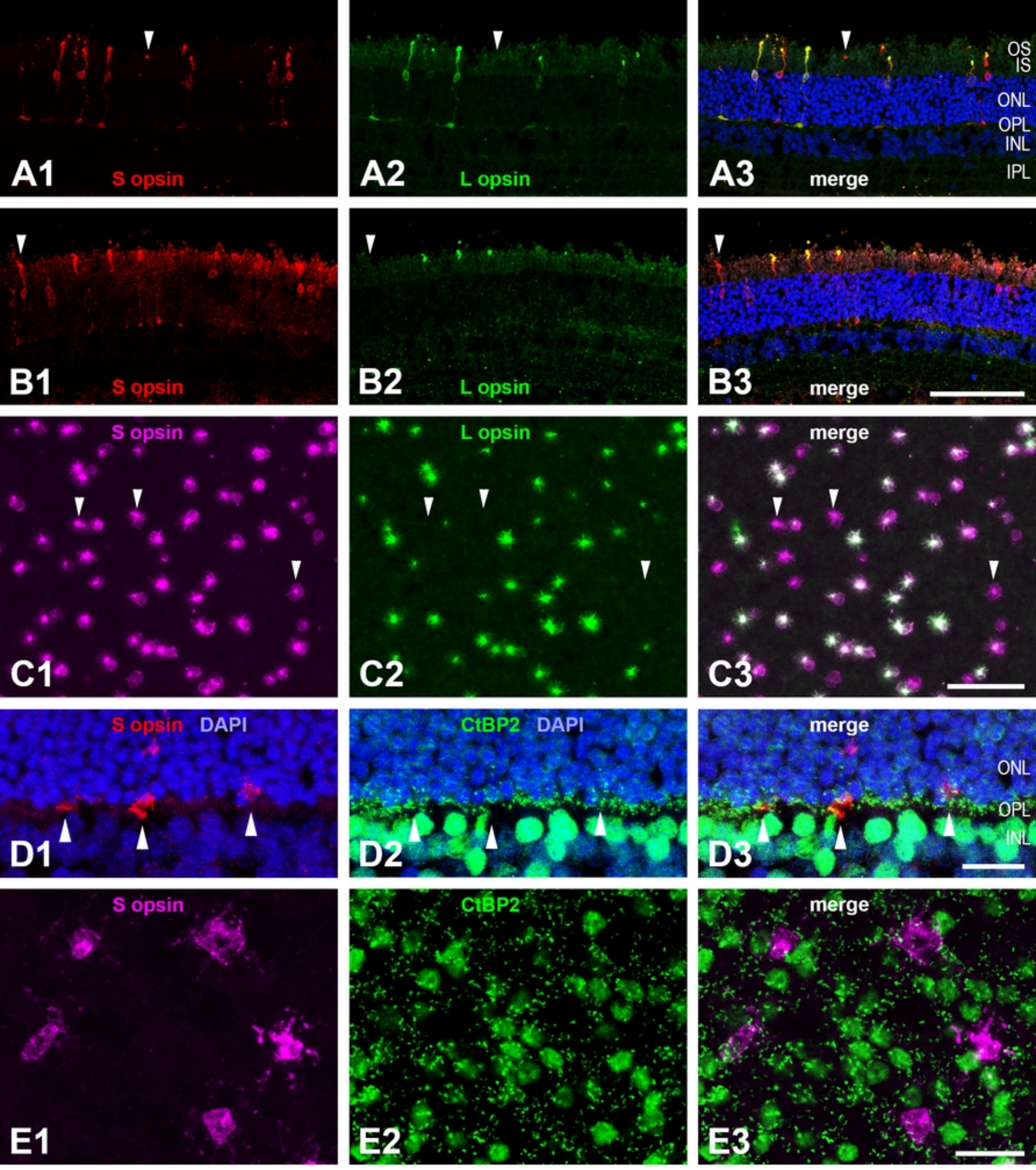
A1
S opsin
A2
L opsin
A3
merge
OS
IS
ONL
OPL
INL
IPL
B1
S opsin
B2
L opsin
B3
merge
C1
S opsin
C2
L opsin
C3
merge
D1
S opsin
DAPI
D2
CtBP2
DAPI
D3
merge
ONL
OPL
INL
E1
S opsin
E2
CtBP2
E3
merge

Figure 6